Martina Bukač* and Catalin Trenchea

Boundary update via resolvent for fluid–structure interaction

https://doi.org/10.1515/jnma-2019-0081
Received August 28, 2019; revised April 22, 2020; accepted May 02, 2020

Abstract: We propose a BOundary Update using Resolvent (BOUR) partitioned method, second-order accurate in time, unconditionally stable, for the interaction between a viscous incompressible fluid and a thin structure. The method is algorithmically similar to the sequential Backward Euler — Forward Euler implementation of the midpoint quadrature rule. (i) The structure and fluid sub-problems are first solved using a Backward Euler scheme, (ii) the velocities of fluid and structure are updated on the boundary via a second-order consistent resolvent operator, and then (iii) the structure and fluid sub-problems are solved again, using a Forward Euler scheme. The stability analysis based on energy estimates shows that the scheme is unconditionally stable. Error analysis of the semi-discrete problem yields second-order convergence in time. The two numerical examples confirm theoretical convergence analysis results and show an excellent agreement between the proposed partitioned scheme and the monolithic scheme.

Keywords: fluid–structure interaction, non-iterative partitioned method, second order accuracy, unconditional stability

Classification: 65M12

1 Introduction

Due to their various applications, development of numerical methods for fluid–structure interaction (FSI) problems has been a subject of extensive research [1, 5–7, 15, 19–22, 24, 28, 33, 37–40, 42]. Computational algorithms for FSI problems can be classified as monolithic or partitioned. In the monolithic approach, the fluid and structure equations are solved together [19, 25, 40]. Using this approach, the two problems remain strongly coupled, but the resulting linear system is large and ill-conditioned [3, 40]. Alternatively, using the partitioned approach, the fluid problem is solved separately from the structure problem, resulting in two smaller and better-conditioned linear systems. Partitioned algorithms can be further classified as strongly-coupled [1, 2, 4, 45], in which case the fluid and structure sub-problems are iteratively solved within one time step until the energy at the interface is balanced, or loosely-coupled [6, 10, 20, 37, 38], when such sub-iterations are not needed. Since the complexity and computational time of strongly coupled partitioned algorithms may often be comparable to a monolithic approach, loosely-coupled schemes have been a popular choice. However, loosely coupled algorithms often suffer from numerical instabilities known as the 'added mass effect', which is apparent in applications, where the fluid and solid densities are similar, such as hemodynamics.

Loosely coupled methods or the interaction between a fluid and a thin structure based on the Lie operator splitting approach were proposed in [11, 12, 20]. The 'kinematically coupled β scheme' introduced in [10, 11] is obtained by adding and subtracting the fluid pressure from the previous time step, while the 'incremental displacement–correction scheme' introduced in [20] is obtained by adding and subtracting the elastic operator applied to the displacement from the previous time step. In both schemes, the fluid sub-problem is solved with a Robin boundary condition which takes into account the structure mass at the fluid–structure interface, exploiting the assumption that the structure is thin, i.e., has lower dimension than the fluid. The incremental

***Corresponding author: Martina Bukač,** Department of Applied and Computational Mathematics and Statistics, University of Notre Dame, Notre Dame, IN 46556, USA. Email: mbukac@nd.edu
Catalin Trenchea, Department of Mathematics, University of Pittsburgh, Pittsburgh, PA 15260, USA.

displacement–correction scheme and the kinematically coupled β scheme for $\beta = 1$ have been shown to be first order convergent in time [11, 20]. In [13, 14] the authors propose partitioned and monolithic approaches for FSI problems based on the Nitsche's penalty method. They consider both thin and thick structure models, which result in FSI problems that are more difficult to decouple. Due to numerical instabilities, the proposed partitioned scheme is stabilized by adding a term which controls the pressure variations at the interface. The splitting error, however, lowers the temporal accuracy of the scheme, which was then corrected by proposing a few defect-correction sub-iterations to achieve an optimal, first order convergence rate.

Second-order partitioned schemes have been proposed in [5, 6, 17, 37, 38]. In particular, a partitioned approach based on the Strang splitting was proposed in [37] to study the interaction between non-Newtonian fluids and thin structures. However, the order of convergence was only investigated in numerical experiments. A staggered scheme for fluid–structure interaction problems was proposed in [17]. The scheme was analyzed on a simplified model problem consisting of an elastic spring, a dashpot and two point masses, and shown to be unconditionally stable and second-order accurate. The application of this method to three-dimensional fluid–structure interaction problems involving incompressible fluids has been numerically investigated. While the method provides accurate approximations for several examples if the time step is small enough, it was noted that the method may not be suitable to simulate blood flow problems. Partitioned algorithms based on the so called added-mass partitioned Robin conditions have been proposed in [5, 6]. Using the von Neumann stability analysis, the authors showed that the algorithm for the interaction between a fluid and a thick, elastic structure proposed in [5] is stable under a condition on the time step which depends on the structure parameters. The algorithm proposed in [6], which involves FSI with structural shells, is weakly stable under a Courant–Friedrichs–Lewy (CFL) condition. Although the numerical results indicate second-order convergence in time, the convergence rates are not analytically derived. A loosely-coupled scheme for the interaction between a fluid and a thin structure based on the Crank–Nicolson time discretization, combined with operator-splitting, was proposed in [38]. In order to achieve stability, the fluid problem is solved with a Robin boundary condition containing structure inertia at the fluid–structure interface, where the fluid stress was added and subtracted to ensure second-order convergence in time. Based on energy estimates, the scheme has been shown to be stable under a CFL condition. The optimal convergence rates have been obtained via both a priori error estimates and numerical results.

In this paper, we propose a novel partitioned algorithm for the interaction between an incompressible, viscous fluid and a thin, elastic structure. As commonly done in the literature, we assume that the fluid is modeled using the Stokes equations, that the structure displacement is infinitesimal and that the fluid–structure interaction problem is linear [5, 11, 13, 20]. The proposed BOUR partitioned algorithm is similar to the sequential Backward Euler (BE) – Forward Euler (FE) implementation of the midpoint quadrature rule. (i) The fluid and structure sub-problems are first solved using a BE scheme, (ii) the velocities of fluid and structure are updated on the boundary via a second-order in time consistent resolvent operator, and then (iii) the structure and fluid sub-problems are solved again, using a FE scheme. The main novelty of the BOUR algorithm is the way in which the interface conditions are combined with the fluid and structure sub-problems, which leads to an unconditionally stable method. Due to the modus operandi used in coupling of the fluid and solid sub-problems, BOUR differs significantly from the numerical scheme we previously developed in [38], which was only conditionally stable. The stability and convergence properties of the semi-discretized scheme are analyzed in Theorems 3.1 and 4.1, yielding the unconditional stability and optimal, second-order convergence in time. We investigated the properties of the proposed method on two numerical examples, and compared the method to the existing ones in the literature. Our results indicate optimal convergence rate of the BOUR method. Furthermore, we observe an excellent comparison between the BOUR method and a monolithic scheme, even in case of large time steps, making the proposed method an appealing alternative to the monolithic scheme.

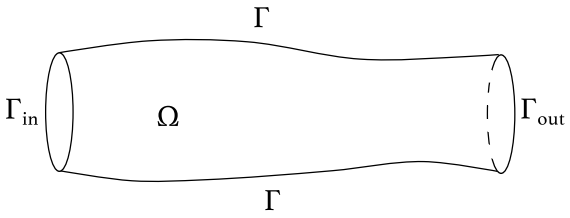

Fig. 1: Fluid domain Ω. The lateral boundary Γ represents an elastic structure.

2 Description of the problem

We are interested in modeling the interaction between a viscous incompressible fluid and a thin elastic structure. We assume that the fluid is occupying domain $\Omega \subset \mathbb{R}^d$, $d = 2, 3$, and that $\partial\Omega = \Gamma \cup \Gamma_{\text{in}} \cup \Gamma_{\text{out}}$, where Γ represents the elastic structure, Γ_{in} represents inflow, and Γ_{out} represents outflow (see Fig. 1). We also assume that the flow is modeled using the Stokes equations for a Newtonian fluid, that the structure undergoes infinitesimal displacements and that the fluid–structure interaction is linear. These are common assumptions in the analysis of partitioned schemes for FSI problems [5, 11, 13, 20].

The fluid equations in a fixed domain Ω are given by

$$\rho_f \partial_t \boldsymbol{u} = \nabla \cdot \boldsymbol{\sigma}(\boldsymbol{u}, p) \quad \text{in } \Omega \times (0, T) \tag{2.1}$$

$$\nabla \cdot \boldsymbol{u} = 0 \qquad \text{in } \Omega \times (0, T) \tag{2.2}$$

$$\boldsymbol{\sigma}(\boldsymbol{u}, p)\boldsymbol{n} = -p_{\text{in}}(t)\boldsymbol{n} \quad \text{on } \Gamma_{\text{in}} \times (0, T) \tag{2.3}$$

$$\boldsymbol{\sigma}(\boldsymbol{u}, p)\boldsymbol{n} = -p_{\text{out}}(t)\boldsymbol{n} \quad \text{on } \Gamma_{\text{out}} \times (0, T) \tag{2.4}$$

$$\boldsymbol{u}(\cdot, 0) = \boldsymbol{u}^0 \qquad \text{in } \Omega \tag{2.5}$$

where $\boldsymbol{u} = (u_i)_{i=1,\dots,d}$ is the fluid velocity, p is the fluid pressure, ρ_f is the fluid density and $\boldsymbol{\sigma}(\boldsymbol{u}, p) = -p\boldsymbol{I} + 2\mu\boldsymbol{D}(\boldsymbol{u})$ is the fluid stress tensor, where $\boldsymbol{D}(\boldsymbol{u}) = (\nabla\boldsymbol{u} + (\nabla\boldsymbol{u})^T)/2$ is the strain rate tensor and μ is the fluid viscosity. The outward normal to the fluid domain boundary is denoted by $\boldsymbol{n}$, while p_{in} and p_{out} are the prescribed inflow and outflow forces, respectively.

The structure elastodynamics is described by a linearly elastic, lower-dimensional model, given by

$$\rho_s h \partial_{tt} \boldsymbol{\eta} + \mathcal{L}_s \boldsymbol{\eta} = \boldsymbol{f} \qquad \text{on } \Gamma \times (0, T) \tag{2.6}$$

$$\boldsymbol{\eta} = \boldsymbol{0} \qquad \text{on } \partial\Gamma \times (0, T) \tag{2.7}$$

$$\boldsymbol{\eta}(\cdot, 0) = \boldsymbol{\eta}^0, \quad \partial_t \boldsymbol{\eta}(\cdot, 0) = \boldsymbol{\eta}_v^0 \quad \text{on } \Gamma \tag{2.8}$$

where $\boldsymbol{\eta} = (\eta_i)_{i=1,\dots,d}$ denotes the structure displacement, ρ_s denotes the structure density, h denotes the structure thickness, and $\boldsymbol{f}$ is a surface force applied by the fluid on the structure. We assume that there are no external forces acting on the structure. The operator $\mathcal{L}_s$ describes the elastic behavior of the structure. Specific choices of $\mathcal{L}_s$ are detailed in Section 5. We define an inner-product associated with the structure operator

$$a_s(\boldsymbol{\eta}, \boldsymbol{\zeta}) = \int_\Gamma \mathcal{L}_s \boldsymbol{\eta} \cdot \boldsymbol{\zeta} \, \mathrm{d}S$$

and norm $\|\boldsymbol{\eta}\|_S^2 = a_s(\boldsymbol{\eta}, \boldsymbol{\eta})$. We assume that operator $\mathcal{L}_s : D(\mathcal{L}_s) \subset H^1(\Gamma) \to H^{-1}(\Gamma)$ is a maximal monotone operator [9], such that a Poincaré type inequality holds

$$\|\boldsymbol{\eta}\|_{L^2(\Gamma)} \leqslant C_{P,S} \|\boldsymbol{\eta}\|_S \tag{2.9}$$

and the norm $\|\cdot\|_S$ is equivalent to the $H^1(\Gamma)$ norm. One example of such an operator is the one associated with the linearly elastic cylindrical Koiter shell used in [12].

To couple the fluid and the structure, we prescribe the kinematic and dynamic coupling conditions. The kinematic coupling condition enforces the continuity of velocities at the fluid–structure interface:

$$\boldsymbol{u} = \partial_t \boldsymbol{\eta} \quad \text{on } \Gamma \times (0, T). \tag{2.10}$$

The dynamic coupling condition enforces the conservation of momentum:

$$\boldsymbol{f} = -\boldsymbol{\sigma}(\boldsymbol{u}, p)\boldsymbol{n} \quad \text{on } \Gamma \times (0, T). \tag{2.11}$$

Equations (2.1)–(2.11) define a linear fluid–structure interaction problem, which has a well-defined energy [11, 38].

3 Numerical scheme

We start by rewriting the coupled problem. Introduce the displacement velocity $\boldsymbol{\xi} = \partial_t \boldsymbol{\eta}$. The coupled problem can be reformulated in the following way: Find $\boldsymbol{u}$, p, $\boldsymbol{\eta}$, and $\boldsymbol{\xi}$ such that

$$\rho_f \partial_t \boldsymbol{u} = \nabla \cdot \boldsymbol{\sigma}(\boldsymbol{u}, p) \quad \text{in } \Omega \times (0, T) \tag{3.1}$$

$$\nabla \cdot \boldsymbol{u} = 0 \qquad \text{in } \Omega \times (0, T) \tag{3.2}$$

$$\rho_s h \partial_t \boldsymbol{\xi} + \mathcal{L}_s \boldsymbol{\eta} = -\boldsymbol{\sigma}(\boldsymbol{u}, p)\boldsymbol{n} \quad \text{on } \Gamma \times (0, T) \tag{3.3}$$

$$\boldsymbol{u} = \boldsymbol{\xi} = \partial_t \boldsymbol{\eta} \quad \text{on } \Gamma \times (0, T) \tag{3.4}$$

with the boundary and initial conditions specified in the previous section.

Let Δt be the time step and $t^n = n\Delta t$ for $n = 0, \dots, N$, where $T = N\Delta t$ is the final time. The proposed, semi-discrete numerical scheme is given as follows.

Algorithm 3.1 (BOUR). Given $\boldsymbol{u}^0$ in Ω, and $\boldsymbol{\eta}^0$, $\boldsymbol{\xi}^0 = \boldsymbol{u}|_\Gamma^0$ on Γ, we first need to compute $\boldsymbol{u}^{1/2}$, $p^{1/2}$, $\boldsymbol{u}^1$ in Ω, and $\boldsymbol{\eta}^{1/2}$, $\boldsymbol{\eta}^1$, $\boldsymbol{\xi}^{1/2}$, $\boldsymbol{\xi}^1$ on Γ with a second-order method. A monolithic method based on a BDF2 or Crank–Nicolson time discretization, or a loosely coupled scheme based on the Crank–Nicolson method proposed in [38] could be used, among others. Then for all $n \geqslant 1$ compute:

$$\text{BE}: \begin{cases} \dfrac{\boldsymbol{\eta}^{n+1/2} - \boldsymbol{\eta}^n}{\Delta t/2} = \boldsymbol{\xi}^{n+1/2} & \text{on } \Gamma \\ \rho_s h \dfrac{\boldsymbol{\xi}^{n+1/2} - \boldsymbol{\xi}^n}{\Delta t/2} + \mathcal{L}_s \boldsymbol{\eta}^{n+1/2} = -\boldsymbol{\sigma}(\boldsymbol{u}^{n-1/2}, p^{n-1/2})\boldsymbol{n} & \text{on } \Gamma \end{cases} \tag{3.5}$$

$$\text{BE}: \begin{cases} \rho_f \dfrac{\boldsymbol{u}^{n+1/2} - \boldsymbol{u}^n}{\Delta t/2} - \nabla \cdot \boldsymbol{\sigma}(\boldsymbol{u}^{n+1/2}, p^{n+1/2}) = 0 & \text{in } \Omega \\ \nabla \cdot \boldsymbol{u}^{n+1/2} = 0 & \text{in } \Omega \\ \rho_s h \dfrac{\boldsymbol{u}^{n+1/2} - \boldsymbol{\xi}^{n+1/2}}{\Delta t/2} + \dfrac{\Delta t}{2} \mathcal{L}_s (\boldsymbol{u}^{n+1/2} - \boldsymbol{\xi}^{n+1/2}) \\ \qquad = 2\big(-\boldsymbol{\sigma}(\boldsymbol{u}^{n+1/2}, p^{n+1/2})\boldsymbol{n} + \boldsymbol{\sigma}(\boldsymbol{u}^{n-1/2}, p^{n-1/2})\boldsymbol{n}\big) & \text{on } \Gamma \end{cases} \tag{3.6}$$

$$\text{FE}: \begin{cases} \dfrac{\boldsymbol{\eta}^{n+1} - \boldsymbol{\eta}^{n+1/2}}{\Delta t/2} = \boldsymbol{u}^{n+1/2} & \text{on } \Gamma \\ \rho_s h \dfrac{\boldsymbol{\xi}^{n+1} - \boldsymbol{u}^{n+1/2}}{\Delta t/2} + \mathcal{L}_s \boldsymbol{\eta}^{n+1/2} = -\boldsymbol{\sigma}(\boldsymbol{u}^{n-1/2}, p^{n-1/2})\boldsymbol{n} & \text{on } \Gamma \end{cases} \tag{3.7}$$

$$\text{FE}: \begin{cases} \rho_f \dfrac{\boldsymbol{u}^{n+1} - \boldsymbol{u}^{n+1/2}}{\Delta t/2} - \nabla \cdot \boldsymbol{\sigma}(\boldsymbol{u}^{n+1/2}, p^{n+1/2}) = 0 & \text{in } \Omega \\ \boldsymbol{u}^{n+1} = \boldsymbol{\xi}^{n+1} & \text{on } \Gamma. \end{cases} \tag{3.8}$$

We note that the fluid BE and FE problems should be complemented with boundary conditions (2.3)–(2.4) evaluated at $t^{n+1/2}$, and the structure BE and FE problems should be solved with structure boundary condition (2.7).

Remark 3.1. Operator $\frac{\rho_s h}{\Delta t} I + \frac{\Delta t}{4}\mathcal{L}_s$ is bijective from $D(\mathcal{L}_s)$ onto $H := L^2(\Gamma)$. Furthermore, $\frac{\Delta t}{\rho_s h}\mathcal{J}$ is the resolvent of $\mathcal{L}_s$ and

$$\mathcal{J} = \left(\frac{\rho_s h}{\Delta t} I + \frac{\Delta t}{4}\mathcal{L}_s\right)^{-1} \tag{3.9}$$

is a bounded operator, with the following bounds on the operator-norms:

$$\|\mathcal{J}\|_{L(H)} \leqslant \frac{\Delta t}{\rho_s h}, \qquad \|\mathcal{L}_s\mathcal{J}\|_{L(H)} \leqslant \frac{\Delta t}{\rho_s h}\|\mathcal{L}_s\|_{L(H)}. \tag{3.10}$$

Note that denoting $\alpha = \frac{\Delta t^2}{4\rho_s h}$, $\mathcal{J}^\alpha = (I + \alpha\mathcal{L}_s)^{-1}$, and $\mathcal{L}_s^\alpha$ the Yosida approximation of $\mathcal{L}_s$, we have

$$\mathcal{L}_s\mathcal{J} = \mathcal{L}_s\left(\frac{\rho_s h}{\Delta t} I + \frac{\Delta t}{4}\mathcal{L}_s\right)^{-1} = \frac{\Delta t}{\rho_s h}\mathcal{L}_s\left(I + \frac{\Delta t^2}{4\rho_s h}\mathcal{L}_s\right)^{-1} \equiv \frac{\Delta t}{\rho_s h}\mathcal{L}_s\mathcal{J}^\alpha \equiv \frac{\Delta t}{\rho_s h}\mathcal{L}_s^\alpha$$

which in turns, due to (see, e.g., [9, Prop. 7.2]):

$$\|\mathcal{L}_s^\alpha(z)\| \leqslant \|\mathcal{L}_s(z)\| \quad \forall z \in D(\mathcal{L}_s)$$

gives the second part of (3.10). Furthermore, the following $\mathcal{J}$-norm is well-defined

$$\begin{aligned}\|\boldsymbol{\eta}\|_{\mathcal{J}}^2 &= (\boldsymbol{\eta}, \underbrace{\mathcal{J}\boldsymbol{\eta}}_{:=\boldsymbol{\nu}}) = \left(\left(\frac{\rho_s h}{\Delta t} I + \frac{\Delta t}{4}\mathcal{L}_s\right)\boldsymbol{\nu}, \boldsymbol{\nu}\right) = \frac{\rho_s h}{\Delta t}\|\boldsymbol{\nu}\|_{L^2(\Gamma)}^2 + \frac{\Delta t}{4}\|\boldsymbol{\nu}\|_S^2 \\ &= \frac{\rho_s h}{\Delta t}\|\mathcal{J}\boldsymbol{\eta}\|_{L^2(\Gamma)}^2 + \frac{\Delta t}{4}\|\mathcal{J}\boldsymbol{\eta}\|_S^2.\end{aligned} \tag{3.11}$$

We also note that the boundary condition in (3.6) can be written as

$$\boldsymbol{u}^{n+1/2} - \boldsymbol{\xi}^{n+1/2} = \mathcal{J}\Big(-\boldsymbol{\sigma}(\boldsymbol{u}^{n+1/2}, p^{n+1/2})\boldsymbol{n} + \boldsymbol{\sigma}(\boldsymbol{u}^{n-1/2}, p^{n-1/2})\boldsymbol{n}\Big). \tag{BOUR}$$

Remark 3.2. Computational savings can be achieved by combining the stages of (3.5)–(3.8), which shows that the proposed numerical scheme is similar to the sequential BE–FE implementation of the midpoint method. Evaluating the first displacement equation in (3.7) at $n-1$ instead of n and adding it to the first displacement equation in (3.5) we get

$$\frac{\boldsymbol{\eta}^{n+1/2} - \boldsymbol{\eta}^{n-1/2}}{\Delta t} = \frac{\boldsymbol{\xi}^{n+1/2} + \boldsymbol{u}^{n-1/2}|_\Gamma}{2} \quad \text{on } \Gamma.$$

Similarly, velocity equations in (3.7) and (3.5) can be combined to obtain

$$\begin{aligned}&\rho_s h\frac{\boldsymbol{\xi}^{n+1/2} - \boldsymbol{u}^{n-1/2}|_\Gamma}{\Delta t} + \mathcal{L}_s\left(\frac{\boldsymbol{\eta}^{n+1/2} + \boldsymbol{\eta}^{n-1/2}}{2}\right) \\ &\quad = -\frac{1}{2}\Big(\boldsymbol{\sigma}(\boldsymbol{u}^{n-1/2}|_\Gamma, p^{n-1/2}|_\Gamma)\boldsymbol{n} + \boldsymbol{\sigma}(\boldsymbol{u}^{n-3/2}|_\Gamma, p^{n-3/2}|_\Gamma)\boldsymbol{n}\Big) \quad \text{on } \Gamma.\end{aligned} \tag{3.12}$$

For the fluid, we again write the first relation in (3.8) at $n-1$ instead of n and add it to the first relation in (3.6) to obtain

$$\rho_f\frac{\boldsymbol{u}^{n+1/2} - \boldsymbol{u}^{n-1/2}}{\Delta t} - \frac{1}{2}\nabla\cdot\Big(\boldsymbol{\sigma}(\boldsymbol{u}^{n+1/2}, p^{n+1/2}) + \boldsymbol{\sigma}(\boldsymbol{u}^{n-1/2}, p^{n-1/2})\Big) = 0 \quad \text{in } \Omega.$$

The boundary conditions on the fluid part at half-integers are given in relation (BOUR), while at the integer values, the relation $\boldsymbol{u}^n = \boldsymbol{\xi}^n$ gives again (3.12). Therefore, the numerical algorithm at half-integer values can be written as

$$\frac{\boldsymbol{\eta}^{n+1/2} - \boldsymbol{\eta}^{n-1/2}}{\Delta t} = \frac{\boldsymbol{\xi}^{n+1/2} + \boldsymbol{u}^{n-1/2}|_\Gamma}{2} \quad \text{on } \Gamma \tag{3.13}$$

$$\begin{aligned}&\rho_s h\frac{\boldsymbol{\xi}^{n+1/2} - \boldsymbol{u}^{n-1/2}|_\Gamma}{\Delta t} + \mathcal{L}_s\Big(\frac{\boldsymbol{\eta}^{n+1/2} + \boldsymbol{\eta}^{n-1/2}}{2}\Big) \\ &\quad = -\frac{1}{2}\Big(\boldsymbol{\sigma}(\boldsymbol{u}^{n-1/2}|_\Gamma, p^{n-1/2}|_\Gamma)\boldsymbol{n} + \boldsymbol{\sigma}(\boldsymbol{u}^{n-3/2}|_\Gamma, p^{n-3/2}|_\Gamma)\boldsymbol{n}\Big) \quad \text{on } \Gamma\end{aligned} \tag{3.14}$$

$$\rho_f\frac{\boldsymbol{u}^{n+1/2} - \boldsymbol{u}^{n-1/2}}{\Delta t} - \frac{1}{2}\nabla\cdot\Big(\boldsymbol{\sigma}(\boldsymbol{u}^{n+1/2}, p^{n+1/2}) + \boldsymbol{\sigma}(\boldsymbol{u}^{n-1/2}, p^{n-1/2})\Big) = 0 \quad \text{in } \Omega \tag{3.15}$$

$$\boldsymbol{u}^{n+1/2} = \boldsymbol{\xi}^{n+1/2} - \mathcal{J}(\boldsymbol{\sigma}(\boldsymbol{u}^{n+1/2}, p^{n+1/2})\boldsymbol{n} - \boldsymbol{\sigma}(\boldsymbol{u}^{n-1/2}, p^{n-1/2})\boldsymbol{n}) \quad \text{on } \Gamma. \tag{3.16}$$

This formulation of the proposed algorithm will be used in the convergence analysis.

Remark 3.3. We point out that Algorithm 3.1 is presented in the sequential implementation BE–FE of the midpoint rule (3.5)–(3.8) for the theoretical argumentation. From a computational viewpoint, the bulk of the work in Algorithm 3.1 is performed in the Backward-Euler (BE) steps, as the Forward-Euler (FE) steps are equivalent to linear extrapolations, acting like time-filters (see, e.g., [29, 30, 35]):

$$
\text{BE}: \begin{cases} \dfrac{\boldsymbol{\eta}^{n+1/2}-\boldsymbol{\eta}^{n}}{\Delta t/2} = \boldsymbol{\xi}^{n+1/2} \quad \text{on } \Gamma \\ \rho_s h \dfrac{\boldsymbol{\xi}^{n+1/2}-\boldsymbol{\xi}^{n}}{\Delta t/2} + \mathcal{L}_s \boldsymbol{\eta}^{n+1/2} = -\boldsymbol{\sigma}(\boldsymbol{u}^{n-1/2}|_\Gamma, p^{n-1/2}|_\Gamma)\boldsymbol{n} \quad \text{on } \Gamma \end{cases}
$$

$$
\text{BE}: \begin{cases} \rho_f \dfrac{\boldsymbol{u}^{n+1/2}-\boldsymbol{u}^{n}}{\Delta t/2} - \nabla\cdot\boldsymbol{\sigma}(\boldsymbol{u}^{n+1/2}, p^{n+1/2}) = 0 \quad \text{in } \Omega \\ \nabla\cdot\boldsymbol{u}^{n+1/2} = 0 \quad \text{in } \Omega \\ \rho_s h \dfrac{\boldsymbol{u}^{n+1/2}-\boldsymbol{\xi}^{n+1/2}}{\Delta t/2} + \dfrac{\Delta t}{2}\mathcal{L}_s(\boldsymbol{u}^{n+1/2}-\boldsymbol{\xi}^{n+1/2}) \\ \qquad = 2\big(-\boldsymbol{\sigma}(\boldsymbol{u}^{n+1/2}, p^{n+1/2})\boldsymbol{n} + \boldsymbol{\sigma}(\boldsymbol{u}^{n-1/2}, p^{n-1/2})\boldsymbol{n}\big) \quad \text{on } \Gamma \end{cases}
$$

$$
\text{FE}: \begin{cases} \boldsymbol{\eta}^{n+1} = 2\boldsymbol{\eta}^{n+1/2} - \boldsymbol{\eta}^{n} + \dfrac{\Delta t}{2}(\boldsymbol{u}^{n+1/2}|_\Gamma - \boldsymbol{\xi}^{n+1/2}) \quad \text{on } \Gamma \\ \boldsymbol{\xi}^{n+1} = \boldsymbol{u}^{n+1/2}|_\Gamma + \boldsymbol{\xi}^{n+1/2} - \boldsymbol{\xi}^{n} \quad \text{on } \Gamma \end{cases}
$$

$$
\text{FE}: \begin{cases} \boldsymbol{u}^{n+1} = 2\boldsymbol{u}^{n+1/2} - \boldsymbol{u}^{n} \quad \text{in } \Omega \\ \boldsymbol{u}^{n+1} = \boldsymbol{\xi}^{n+1} \quad \text{on } \Gamma. \end{cases}
$$

3.1 Stability and energy estimates

Denote by $\mathcal{E}_s^N$ is the sum of the elastic energy of the structure, kinetic energy of the structure, and kinetic energy of the fluid

$$
\mathcal{E}_s^N = \frac{1}{2}\|\boldsymbol{\eta}^N\|_S^2 + \frac{\rho_s h}{2}\|\boldsymbol{\xi}^N\|_{L^2(\Gamma)}^2 + \frac{\rho_f}{2}\|\boldsymbol{u}^N\|_{L^2(\Omega)}^2
$$

and by $\mathcal{D}_s^N$ is the fluid viscous dissipation rate

$$
\mathcal{D}_s^N = 2\mu\Delta t\sum_{n=1}^{N-1}\|\boldsymbol{D}(\boldsymbol{u}^{n+1/2})\|_{L^2(\Omega)}^2.
$$

The stability of the scheme (3.5)–(3.8) is given in the following theorem.

Theorem 3.1. *Assume that the system is isolated, i.e., $p_{\text{in}} = p_{\text{out}} = 0$, and that $a_s(\cdot,\cdot)$ is an inner-product associated with the structure operator $\mathcal{L}_s$. We also assume that $\mathcal{L}_s$ is a maximal monotone operator, such that inequality* (2.9) *holds, the norm $\|\boldsymbol{\eta}\|_S = (a_s(\boldsymbol{\eta},\boldsymbol{\eta}))^{1/2}$ is equivalent to the $H^1(\Gamma)$ norm, and $\frac{\Delta t}{\rho_s h}\mathcal{J}$ is the resolvent of $\mathcal{L}_s$. Let $(\boldsymbol{\xi}^n, \boldsymbol{\eta}^n, \boldsymbol{u}^n, p^n)$ be the solution of* (3.5)–(3.8)*. Then, the following a priori energy equality holds*

$$
\mathcal{E}_s^N + \mathcal{D}_s^N + \mathcal{N}_s^N = \mathcal{E}_s^1 + \frac{\Delta t}{4}\big\|\boldsymbol{\sigma}(\boldsymbol{u}^{1/2}|_\Gamma, p^{1/2}|_\Gamma)\boldsymbol{n}\big\|_{\mathcal{J}}^2
$$

where $\mathcal{N}_s^N$ denotes terms due to numerical dissipation

$$
\mathcal{N}_s^N = \frac{\Delta t}{4}\big\|\boldsymbol{\sigma}(\boldsymbol{u}^{N+1/2}|_\Gamma, p^{N+1/2}|_\Gamma)\boldsymbol{n}\big\|_{\mathcal{J}}^2 + \frac{\rho_s h}{4}\sum_{n=1}^{N-1}\|\boldsymbol{u}^{n+1/2}-\boldsymbol{\xi}^{n+1/2}\|_{L^2(\Gamma)}^2 + \frac{\Delta t^2}{16}\sum_{n=1}^{N-1}\|\boldsymbol{u}^{n+1/2}-\boldsymbol{\xi}^{n+1/2}\|_S^2.
$$

Proof. We multiply (3.5) by $\mathcal{L}_s\boldsymbol{\eta}^{n+1/2}$ and $\boldsymbol{\xi}^{n+1/2}$, respectively, integrate over Γ, add and apply the polarized identity $(a-b)a = \frac{1}{2}a^2 - \frac{1}{2}b^2 + \frac{1}{2}(a-b)^2$ to obtain:

$$\begin{aligned}0 = &\frac{1}{\Delta t}\Big(\|\boldsymbol{\eta}^{n+1/2}\|_S^2 - \|\boldsymbol{\eta}^n\|_S^2 + \|\boldsymbol{\eta}^{n+1/2} - \boldsymbol{\eta}^n\|_S^2\Big)\\ &+ \frac{\rho_s h}{\Delta t}\Big(\|\boldsymbol{\xi}^{n+1/2}\|_{L^2(\Gamma)}^2 - \|\boldsymbol{\xi}^n\|_{L^2(\Gamma)}^2 + \|\boldsymbol{\xi}^{n+1/2} - \boldsymbol{\xi}^n\|_{L^2(\Gamma)}^2\Big) + \int_\Gamma \boldsymbol{\sigma}(\boldsymbol{u}^{n-1/2}|_\Gamma, p^{n-1/2}|_\Gamma)\boldsymbol{n}\,\boldsymbol{\xi}^{n+1/2}.\end{aligned}$$

Similarly, from (3.7), multiplying with $\mathcal{L}_s\boldsymbol{\eta}^{n+1/2}$ and $\boldsymbol{u}^{n+1/2}|_\Gamma$, we derive

$$\begin{aligned}0 = &\frac{1}{\Delta t}\Big(\|\boldsymbol{\eta}^{n+1}\|_S^2 - \|\boldsymbol{\eta}^{n+1/2}\|_S^2 - \|\boldsymbol{\eta}^{n+1} - \boldsymbol{\eta}^{n+1/2}\|_S^2\Big)\\ &+ \frac{\rho_s h}{\Delta t}\Big(\|\boldsymbol{\xi}^{n+1}\|_{L^2(\Gamma)}^2 - \|\boldsymbol{u}^{n+1/2}\|_{L^2(\Gamma)}^2 - \|\boldsymbol{\xi}^{n+1} - \boldsymbol{u}^{n+1/2}\|_{L^2(\Gamma)}^2\Big) + \int_\Gamma \boldsymbol{\sigma}(\boldsymbol{u}^{n-1/2}|_\Gamma, p^{n-1/2}|_\Gamma)\boldsymbol{n}\,\boldsymbol{u}^{n+1/2}|_\Gamma.\end{aligned}$$

Hence, from the structure part, we have

$$\begin{aligned}0 = &\frac{1}{\Delta t}\Big(\|\boldsymbol{\eta}^{n+1}\|_S^2 - \|\boldsymbol{\eta}^n\|_S^2 - \|\boldsymbol{\eta}^{n+1} - \boldsymbol{\eta}^{n+1/2}\|_S^2 + \|\boldsymbol{\eta}^{n+1/2} - \boldsymbol{\eta}^n\|_S^2\Big)\\ &+ \frac{\rho_s h}{\Delta t}\Big(\|\boldsymbol{\xi}^{n+1}\|_{L^2(\Gamma)}^2 - \|\boldsymbol{\xi}^n\|_{L^2(\Gamma)}^2 + \|\boldsymbol{\xi}^{n+1/2}\|_{L^2(\Gamma)}^2 - \|\boldsymbol{u}^{n+1/2}\|_{L^2(\Gamma)}^2\Big)\\ &+ \frac{\rho_s h}{\Delta t}\left(\|\boldsymbol{\xi}^{n+1/2} - \boldsymbol{\xi}^n\|_{L^2(\Gamma)}^2 - \|\boldsymbol{\xi}^{n+1} - \boldsymbol{u}^{n+1/2}\|_{L^2(\Gamma)}^2\right) + \int_\Gamma \boldsymbol{\sigma}(\boldsymbol{u}^{n-1/2}|_\Gamma, p^{n-1/2}|_\Gamma)\boldsymbol{n}\,(\boldsymbol{\xi}^{n+1/2} + \boldsymbol{u}^{n+1/2}).\end{aligned}$$

Using again the displacement equations in (3.7) and (3.5) we have

$$-\|\boldsymbol{\eta}^{n+1} - \boldsymbol{\eta}^{n+1/2}\|_S^2 + \|\boldsymbol{\eta}^{n+1/2} - \boldsymbol{\eta}^n\|_S^2 = \frac{\Delta t^2}{4}\Big(-\|\boldsymbol{u}^{n+1/2}\|_S^2 + \|\boldsymbol{\xi}^{n+1/2}\|_S^2\Big)$$

while the velocity equations yield

$$-\|\boldsymbol{\xi}^{n+1} - \boldsymbol{u}^{n+1/2}\|_{L^2(\Gamma)}^2 + \|\boldsymbol{\xi}^{n+1/2} - \boldsymbol{\xi}^n\|_{L^2(\Gamma)}^2 = 0.$$

Hence the above energy estimate on the structure part gives

$$\begin{aligned}0 = &\frac{1}{\Delta t}\Big(\|\boldsymbol{\eta}^{n+1}\|_S^2 - \|\boldsymbol{\eta}^n\|_S^2\Big)\\ &+ \frac{\rho_s h}{\Delta t}\Big(\|\boldsymbol{\xi}^{n+1}\|_{L^2(\Gamma)}^2 - \|\boldsymbol{\xi}^n\|_{L^2(\Gamma)}^2\Big) + \frac{\rho_s h}{\Delta t}\Big(\|\boldsymbol{\xi}^{n+1/2}\|_{L^2(\Gamma)}^2 - \|\boldsymbol{u}^{n+1/2}\|_{L^2(\Gamma)}^2\Big)\\ &+ \frac{\Delta t}{4}\Big(-\|\boldsymbol{u}^{n+1/2}\|_S^2 + \|\boldsymbol{\xi}^{n+1/2}\|_S^2\Big) + \int_\Gamma \boldsymbol{\sigma}(\boldsymbol{u}^{n-1/2}|_\Gamma, p^{n-1/2}|_\Gamma)\boldsymbol{n}\,(\boldsymbol{\xi}^{n+1/2} + \boldsymbol{u}^{n+1/2}).\end{aligned} \tag{3.17}$$

For the fluid part, we multiply the first two equations in (3.6) by $\boldsymbol{u}^{n+1/2}$ and $2p^{n+1/2}$ respectively, and (3.8) by $\boldsymbol{u}^{n+1/2}$, integrate over Ω, add and obtain

$$\begin{aligned}0 = &\frac{\rho_f}{\Delta t}\Big(\|\boldsymbol{u}^{n+1}\|_{L^2(\Omega)}^2 - \|\boldsymbol{u}^n\|_{L^2(\Omega)}^2 - \|\boldsymbol{u}^{n+1} - \boldsymbol{u}^{n+1/2}\|_{L^2(\Omega)}^2 + \|\boldsymbol{u}^{n+1/2} - \boldsymbol{u}^n\|_{L^2(\Omega)}^2\Big)\\ &- 2\int_\Gamma \boldsymbol{\sigma}(\boldsymbol{u}^{n-1/2}|_\Gamma, p^{n-1/2}|_\Gamma)\boldsymbol{n}\,\boldsymbol{u}^{n+1/2} + 2\int_\Omega \boldsymbol{\sigma}(\boldsymbol{u}^{n+1/2}, p^{n+1/2}) : \nabla\boldsymbol{u}^{n+1/2}\\ &+ \frac{\rho_s h}{\Delta t}\Big(\|\boldsymbol{u}^{n+1/2}\|_{L^2(\Gamma)}^2 - \|\boldsymbol{\xi}^{n+1/2}\|_{L^2(\Gamma)}^2 + \|\boldsymbol{u}^{n+1/2} - \boldsymbol{\xi}^{n+1/2}\|_{L^2(\Gamma)}^2\Big)\\ &+ \frac{\Delta t}{4}\|\boldsymbol{u}^{n+1/2}\|_S^2 - \frac{\Delta t}{4}\|\boldsymbol{\xi}^{n+1/2}\|_S^2 + \frac{\Delta t}{4}\|\boldsymbol{u}^{n+1/2} - \boldsymbol{\xi}^{n+1/2}\|_S^2 + 2\int_\Omega p^{n+1/2}\nabla\cdot\boldsymbol{u}^{n+1/2}.\end{aligned}$$

Taking into account the flow equations we have

$$-\|\boldsymbol{u}^{n+1} - \boldsymbol{u}^{n+1/2}\|_{L^2(\Omega)}^2 + \|\boldsymbol{u}^{n+1/2} - \boldsymbol{u}^n\|_{L^2(\Omega)}^2 = 0.$$

Hence the fluid part of the energy estimates gives

$$\begin{aligned}0 = &\frac{\rho_f}{\Delta t}\Big(\|\boldsymbol{u}^{n+1}\|_{L^2(\Omega)}^2 - \|\boldsymbol{u}^n\|_{L^2(\Omega)}^2\Big) + 4\mu\|\boldsymbol{D}(\boldsymbol{u}^{n+1/2})\|_{L^2(\Omega)}^2\\ &+ \frac{\rho_s h}{\Delta t}\Big(\|\boldsymbol{u}^{n+1/2}\|_{L^2(\Gamma)}^2 - \|\boldsymbol{\xi}^{n+1/2}\|_{L^2(\Gamma)}^2 + \|\boldsymbol{u}^{n+1/2} - \boldsymbol{\xi}^{n+1/2}\|_{L^2(\Gamma)}^2\Big)\\ &+ \frac{\Delta t}{4}\|\boldsymbol{u}^{n+1/2}\|_S^2 - \frac{\Delta t}{4}\|\boldsymbol{\xi}^{n+1/2}\|_S^2 + \frac{\Delta t}{4}\|\boldsymbol{u}^{n+1/2} - \boldsymbol{\xi}^{n+1/2}\|_S^2 - 2\int_\Gamma \boldsymbol{\sigma}(\boldsymbol{u}^{n-1/2}|_\Gamma, p^{n-1/2}|_\Gamma)\boldsymbol{n}\,\boldsymbol{u}^{n+1/2}|_\Gamma.\end{aligned}$$

Therefore the structure and fluid estimates combine to give

$$
\begin{aligned}
0 = {} & \frac{1}{\Delta t}\Big(\|\boldsymbol{\eta}^{n+1}\|_S^2 - \|\boldsymbol{\eta}^{n}\|_S^2\Big) + \frac{\rho_s h}{\Delta t}\Big(\|\boldsymbol{\xi}^{n+1}\|_{L^2(\Gamma)}^2 - \|\boldsymbol{\xi}^{n}\|_{L^2(\Gamma)}^2\Big) \\
& + \frac{\rho_s h}{\Delta t}\|\boldsymbol{u}^{n+1/2} - \boldsymbol{\xi}^{n+1/2}\|_{L^2(\Gamma)}^2 + \frac{\Delta t}{4}\|\boldsymbol{u}^{n+1/2} - \boldsymbol{\xi}^{n+1/2}\|_S^2 \\
& + \frac{\rho_f}{\Delta t}\Big(\|\boldsymbol{u}^{n+1}\|_{L^2(\Omega)}^2 - \|\boldsymbol{u}^{n}\|_{L^2(\Omega)}^2\Big) + 4\mu\|\boldsymbol{D}(\boldsymbol{u}^{n+1/2})\|_{L^2(\Omega)}^2 + \int_\Gamma \boldsymbol{\sigma}(\boldsymbol{u}^{n-1/2}|_\Gamma, p^{n-1/2}|_\Gamma)\boldsymbol{n}\,(\boldsymbol{\xi}^{n+1/2}|_\Gamma - \boldsymbol{u}^{n+1/2}|_\Gamma).
\end{aligned}
$$

Now using the $\mathcal{J}$-norm (3.11), and the boundary conditions on the fluid part (BOUR) at the half-integer time-steps, we have

$$
\begin{aligned}
& \int_\Gamma \boldsymbol{\sigma}(\boldsymbol{u}^{n-1/2}|_\Gamma, p^{n-1/2}|_\Gamma)\boldsymbol{n}\,(\boldsymbol{\xi}^{n+1/2}|_\Gamma - \boldsymbol{u}^{n+1/2}|_\Gamma) \\
& \qquad = \int_\Gamma \boldsymbol{\sigma}(\boldsymbol{u}^{n-1/2}|_\Gamma, p^{n-1/2}|_\Gamma)\boldsymbol{n}\,\mathcal{J}\Big(\boldsymbol{\sigma}(\boldsymbol{u}^{n+1/2}|_\Gamma, p^{n+1/2}|_\Gamma)\boldsymbol{n} - \boldsymbol{\sigma}(\boldsymbol{u}^{n-1/2}|_\Gamma, p^{n-1/2}|_\Gamma)\boldsymbol{n}\Big) \\
& \qquad = \frac{1}{2}\big\|\boldsymbol{\sigma}(\boldsymbol{u}^{n+1/2}|_\Gamma, p^{n+1/2}|_\Gamma)\boldsymbol{n}\big\|_{\mathcal{J}}^2 - \big\|\boldsymbol{\sigma}(\boldsymbol{u}^{n-1/2}|_\Gamma, p^{n-1/2}|_\Gamma)\boldsymbol{n}\big\|_{\mathcal{J}}^2 \\
& \qquad\quad - \frac{1}{2}\Big\|\boldsymbol{\sigma}(\boldsymbol{u}^{n+1/2}|_\Gamma, p^{n+1/2}|_\Gamma)\boldsymbol{n} - \boldsymbol{\sigma}(\boldsymbol{u}^{n-1/2}|_\Gamma, p^{n-1/2}|_\Gamma)\boldsymbol{n}\Big\|_{\mathcal{J}}^2 \\
& \qquad = \frac{1}{2}\big\|\boldsymbol{\sigma}(\boldsymbol{u}^{n+1/2}|_\Gamma, p^{n+1/2}|_\Gamma)\boldsymbol{n}\big\|_{\mathcal{J}}^2 - \big\|\boldsymbol{\sigma}(\boldsymbol{u}^{n-1/2}|_\Gamma, p^{n-1/2}|_\Gamma)\boldsymbol{n}\big\|_{\mathcal{J}}^2 \\
& \qquad\quad - \frac{\rho_s h}{2\Delta t}\|\boldsymbol{u}^{n+1/2} - \boldsymbol{\xi}^{n+1/2}\|_{L^2(\Gamma)}^2 - \frac{\Delta t}{8}\|\boldsymbol{u}^{n+1/2} - \boldsymbol{\xi}^{n+1/2}\|_S^2.
\end{aligned}
$$

Finally,

$$
\begin{aligned}
0 = {} & \frac{1}{\Delta t}\Big(\|\boldsymbol{\eta}^{n+1}\|_S^2 - \|\boldsymbol{\eta}^{n}\|_S^2\Big) + \frac{\rho_s h}{\Delta t}\Big(\|\boldsymbol{\xi}^{n+1}\|_{L^2(\Gamma)}^2 - \|\boldsymbol{\xi}^{n}\|_{L^2(\Gamma)}^2\Big) \\
& + \frac{\rho_s h}{2\Delta t}\|\boldsymbol{u}^{n+1/2} - \boldsymbol{\xi}^{n+1/2}\|_{L^2(\Gamma)}^2 + \frac{\Delta t}{8}\|\boldsymbol{u}^{n+1/2} - \boldsymbol{\xi}^{n+1/2}\|_S^2 + \frac{\rho_f}{\Delta t}\Big(\|\boldsymbol{u}^{n+1}\|_{L^2(\Omega)}^2 - \|\boldsymbol{u}^{n}\|_{L^2(\Omega)}^2\Big) \\
& + 4\mu\|\boldsymbol{D}(\boldsymbol{u}^{n+1/2})\|_{L^2(\Omega)}^2 + \frac{1}{2}\Big(\big\|\boldsymbol{\sigma}(\boldsymbol{u}^{n+1/2}|_\Gamma, p^{n+1/2}|_\Gamma)\boldsymbol{n}\big\|_{\mathcal{J}}^2 - \big\|\boldsymbol{\sigma}(\boldsymbol{u}^{n-1/2}|_\Gamma, p^{n-1/2}|_\Gamma)\boldsymbol{n}\big\|_{\mathcal{J}}^2\Big).
\end{aligned}
$$

Summation from $n = 1$ to $N - 1$ and multiplication by $\frac{1}{2}\Delta t$ yields

$$
\mathcal{E}_s^N + \mathcal{D}_s^N + \mathcal{N}_s^N = \mathcal{E}_s^1 + \frac{\Delta t}{4}\big\|\boldsymbol{\sigma}(\boldsymbol{u}^{1/2}|_\Gamma, p^{1/2}|_\Gamma)\boldsymbol{n}\big\|_{\mathcal{J}}^2
$$

which completes the proof. □

Remark 3.4. When the system is not isolated, the boundary terms associated with (2.3)–(2.4) can be easily bounded using Young's inequality and the fluid viscous dissipation (see, e.g., [11]) leading to an energy inequality.

4 Error analysis

In this section we analyze the error of the proposed numerical method in time. The process of the analysis is summarized as follows. Using Taylor expansions, we compute the local truncation error, and after some manipulations involving the bound (3.10) on the norm of the linear operator $\mathcal{J}$, we conclude that the method (3.5)–(3.8) is consistent of order 2.

The analysis is based on the notion of modified equations, related to the idea of backward error analysis and geometric integration (see, e.g., [26, 27, 31, 32, 41] and references therein). Instead of regarding the computed values $\boldsymbol{\eta}^n$, $\boldsymbol{\xi}^n$, $\boldsymbol{u}^n$, p^n of (3.5)–(3.8) as approximations to the solutions $\boldsymbol{\eta}(t^n)$, $\boldsymbol{\xi}(t^n)$, $\boldsymbol{u}(t^n)$, $p(t^n)$ of (3.1)–(3.4), we consider them as the solutions to a 'nearby' problem. Namely, we shall construct new partial differential equations (4.13)–(4.17) such that the method (3.5)–(3.8) has cubic consistency order

$\mathcal{O}(\Delta t^3)$ to the modified equations, compared to only quadratic consistency order $\mathcal{O}(\Delta t^2)$ to the original equations (3.1)–(3.4). Let $\boldsymbol{d}$ denote the displacement, $\boldsymbol{w}$ the structure velocity, $\boldsymbol{v}$ the fluid velocity, and q the fluid pressure, such that $(\boldsymbol{d}(t), \boldsymbol{w}(t), \boldsymbol{v}(t), q(t))$ satisfy the modified equations. Since, for example, $\boldsymbol{\eta}(t^n) - \boldsymbol{\eta}^n = (\boldsymbol{\eta}(t^n) - \boldsymbol{d}(t^n)) + (\boldsymbol{d}(t^n) - \boldsymbol{\eta}^n) = (\boldsymbol{\eta}(t^n) - \boldsymbol{d}(t^n)) + \mathcal{O}(\Delta t^3)$, the global errors can hence be characterized by the differences between the solutions $\boldsymbol{\eta}(t^n) - \boldsymbol{d}(t^n)$ of the original and modified equations, respectively. Theorem 4.1 shows that the two manifolds $(\boldsymbol{\eta}(t), \boldsymbol{\xi}(t), \boldsymbol{u}(t), p(t))$ and $(\boldsymbol{d}(t), \boldsymbol{w}(t), \boldsymbol{v}(t), q(t))$ are $\mathcal{O}(\Delta t^2)$ apart.

Assumption 4.1. We assume that the solution $\boldsymbol{\eta}, \boldsymbol{\xi}, \boldsymbol{u}, p$ of (3.1)–(3.4) satisfies the following regularity

$$\begin{gathered}
\boldsymbol{\eta} \in (W^{3,2}(0, T; H^1(\Gamma)))^d, \qquad \boldsymbol{\xi} \in (W^{2,2}(0, T; H^2(\Gamma)))^d \\
\boldsymbol{u} \in (W^{3,2}(0, T; L^2(\Omega)))^d \cap (W^{2,2}(0, T; H^2(\Omega)))^d \cap (W^{1,2}(0, T; H^3(\Gamma)))^d \\
\cap (W^{3,2}(0, T; L^2(\Gamma)))^d \cap (W^{2,2}(0, T; H^1(\Gamma)))^d \\
p \in W^{2,2}(0, T; H^1(\Omega)) \cap W^{1,2}(0, T : H^2(\Gamma)) \cap W^{1,\infty}(0, T; H^1(\Gamma)).
\end{gathered}$$

For the purposes of analysis, we use the half-integer formulation of the proposed method (3.13)–(3.16). In the first part of the analysis, we manipulate the local truncation error to obtain the modified equations related to our numerical scheme. To simplify the presentation, we will assume that the functions typeset without a time argument are evaluated at t^n.

We expand $\boldsymbol{\eta}$, $\boldsymbol{\xi}$, and $\boldsymbol{u}$ about $t = t^n$, evaluate the expansions at $t = t^{n+1/2}$ and $t = t^{n-1/2}$, and plug them in (3.13)–(3.16), obtaining

$$\boldsymbol{\eta}' + \frac{\Delta t^2}{24}\boldsymbol{\eta}''' = \frac{\boldsymbol{\xi} + \boldsymbol{u}}{2} + \frac{\Delta t}{4}(\boldsymbol{\xi}' - \boldsymbol{u}') + \frac{\Delta t^2}{16}(\boldsymbol{\xi}'' + \boldsymbol{u}'') + \frac{\Delta t^3}{96}(\boldsymbol{\xi}''' - \boldsymbol{u}''') + \mathcal{O}(\Delta t^4) \quad \text{on } \Gamma \tag{4.1}$$

$$\begin{aligned}
\frac{\rho_s h}{\Delta t}\Big(\boldsymbol{\xi} - \boldsymbol{u} + \frac{\Delta t}{2}(\boldsymbol{\xi}' + \boldsymbol{u}') + \frac{\Delta t^2}{8}(\boldsymbol{\xi}'' - \boldsymbol{u}'')\Big) + \frac{\Delta t^3}{48}(\boldsymbol{\xi}''' + \boldsymbol{u}''') + \mathcal{L}_s\Big(\boldsymbol{\eta} + \frac{\Delta t^2}{8}\boldsymbol{\eta}''\Big) \\
= -\Big(\boldsymbol{\sigma}(\boldsymbol{u}, p)\boldsymbol{n} - \Delta t\boldsymbol{\sigma}(\boldsymbol{u}', p')\boldsymbol{n} + \frac{5}{8}\Delta t^2\boldsymbol{\sigma}(\boldsymbol{u}'', p'')\boldsymbol{n}\Big) + \frac{7}{24}\Delta t^3\boldsymbol{\sigma}(\boldsymbol{u}''', p''')\boldsymbol{n} + \mathcal{O}(\Delta t^4) \quad \text{on } \Gamma
\end{aligned} \tag{4.2}$$

$$\rho_f\boldsymbol{u}' + \frac{\Delta t^2}{24}\rho_f\boldsymbol{u}''' - \nabla\cdot\boldsymbol{\sigma}(\boldsymbol{u}, p) - \frac{\Delta t^2}{8}\nabla\cdot\boldsymbol{\sigma}(\boldsymbol{u}'', p'') = \mathcal{O}(\Delta t^4) \quad \text{in } \Omega \tag{4.3}$$

$$\nabla\cdot\boldsymbol{u} + \frac{\Delta t}{2}\nabla\cdot\boldsymbol{u}' + \frac{\Delta t^2}{8}\nabla\cdot\boldsymbol{u}'' = \mathcal{O}(\Delta t^3) \quad \text{in } \Omega \tag{4.4}$$

$$\boldsymbol{u} + \frac{\Delta t}{2}\boldsymbol{u}' + \frac{\Delta t^2}{8}\boldsymbol{u}'' + \frac{\Delta t^3}{48}\boldsymbol{u}''' = \boldsymbol{\xi} + \frac{\Delta t}{2}\boldsymbol{\xi}' + \frac{\Delta t^2}{8}\boldsymbol{\xi}'' + \frac{\Delta t^3}{48}\boldsymbol{\xi}''' - \Delta t\mathcal{J}(\boldsymbol{\sigma}(\boldsymbol{u}', p')\boldsymbol{n}) + \mathcal{O}(\Delta t^4) \quad \text{on } \Gamma. \tag{4.5}$$

We first differentiate equation (4.4) to obtain

$$\begin{aligned}
\nabla\cdot\boldsymbol{u}' &= -\frac{\Delta t}{2}\nabla\cdot\boldsymbol{u}'' + \mathcal{O}(\Delta t^2) \quad \text{in } \Omega \\
\nabla\cdot\boldsymbol{u}'' &= -\frac{\Delta t}{2}\nabla\cdot\boldsymbol{u}''' + \mathcal{O}(\Delta t^2) \quad \text{in } \Omega.
\end{aligned}$$

Taking into account latter equations, (4.4) becomes

$$\nabla\cdot\boldsymbol{u} = \mathcal{O}(\Delta t^3) \quad \text{in } \Omega.$$

Rearranging, equation (4.5) can be written as

$$\boldsymbol{\xi} - \boldsymbol{u} = \frac{\Delta t}{2}(\boldsymbol{u}' - \boldsymbol{\xi}') + \frac{\Delta t^2}{8}(\boldsymbol{u}'' - \boldsymbol{\xi}'') + \frac{\Delta t^3}{48}(\boldsymbol{u}''' - \boldsymbol{\xi}''') + \Delta t\mathcal{J}(\boldsymbol{\sigma}(\boldsymbol{u}', p')\boldsymbol{n}) + \mathcal{O}(\Delta t^4). \tag{4.6}$$

By differentiation, we have

$$\boldsymbol{\xi}' - \boldsymbol{u}' = \frac{\Delta t}{2}(\boldsymbol{u}'' - \boldsymbol{\xi}'') + \frac{\Delta t^2}{8}(\boldsymbol{u}''' - \boldsymbol{\xi}''') + \frac{\Delta t^3}{48}(\boldsymbol{u}^{(iv)} - \boldsymbol{\xi}^{(iv)}) + \Delta t\mathcal{J}(\boldsymbol{\sigma}(\boldsymbol{u}'', p'')\boldsymbol{n}) + \mathcal{O}(\Delta t^4) \tag{4.7}$$

$$\boldsymbol{\xi}'' - \boldsymbol{u}'' = \frac{\Delta t}{2}(\boldsymbol{u}''' - \boldsymbol{\xi}''') + \frac{\Delta t^2}{8}(\boldsymbol{u}^{(iv)} - \boldsymbol{\xi}^{(iv)}) + \Delta t\mathcal{J}(\boldsymbol{\sigma}(\boldsymbol{u}''', p''')\boldsymbol{n}) + \mathcal{O}(\Delta t^3). \tag{4.8}$$

Substituting (4.6) in (4.1) and (4.2), after simplifications and rearrangements, we obtain the following local truncation error

$$\begin{aligned}
\boldsymbol{\eta}' &= \boldsymbol{\xi} + \frac{\Delta t}{2}(\boldsymbol{\xi}' - \boldsymbol{u}') + \frac{\Delta t^2}{8}\boldsymbol{\xi}'' - \frac{\Delta t^2}{24}\boldsymbol{\eta}''' + \frac{\Delta t^3}{48}(\boldsymbol{\xi}''' - \boldsymbol{u}''') - \frac{\Delta t}{2}\mathcal{J}(\boldsymbol{\sigma}(\boldsymbol{u}', p')\boldsymbol{n}) + \mathcal{O}(\Delta t^4) \quad \text{on } \Gamma \\
\rho_s h\Big(\boldsymbol{u}' &+ \frac{\Delta t^2}{24}\boldsymbol{u}''' + \mathcal{J}(\boldsymbol{\sigma}(\boldsymbol{u}', p')\boldsymbol{n}\Big) + \mathcal{L}_s\boldsymbol{\eta} + \frac{\Delta t^2}{8}\mathcal{L}_s\boldsymbol{\eta}'' \\
&= -\boldsymbol{\sigma}(\boldsymbol{u}, p)\boldsymbol{n} + \Delta t\boldsymbol{\sigma}(\boldsymbol{u}', p')\boldsymbol{n} - \frac{5}{8}\Delta t^2\boldsymbol{\sigma}(\boldsymbol{u}'', p'')\boldsymbol{n} + \frac{7}{24}\Delta t^3\boldsymbol{\sigma}(\boldsymbol{u}''', p''')\boldsymbol{n} + \mathcal{O}(\Delta t^4) \quad \text{on } \Gamma \\
\rho_f\boldsymbol{u}' - \nabla\cdot\boldsymbol{\sigma}(\boldsymbol{u}, p) &= -\frac{\Delta t^2}{24}\rho_f\boldsymbol{u}''' + \frac{\Delta t^2}{8}\nabla\cdot\boldsymbol{\sigma}(\boldsymbol{u}'', p'') + \mathcal{O}(\Delta t^4) \quad \text{in } \Omega \\
\boldsymbol{u} &= \boldsymbol{\xi} + \frac{\Delta t}{2}(\boldsymbol{\xi}' - \boldsymbol{u}') + \frac{\Delta t^2}{8}(\boldsymbol{\xi}'' - \boldsymbol{u}'') + \frac{\Delta t^3}{48}(\boldsymbol{\xi}''' - \boldsymbol{u}''') \\
&\quad - \Delta t\mathcal{J}(\boldsymbol{\sigma}(\boldsymbol{u}', p')\boldsymbol{n}) + \mathcal{O}(\Delta t^4) \quad \text{on } \Gamma.
\end{aligned}$$

Using (4.7) in the first and last equations, applying (3.10) and rearranging we get

$$\begin{aligned}
\boldsymbol{\eta}' &= \boldsymbol{\xi} + \frac{\Delta t^2}{4}(\boldsymbol{u}'' - \boldsymbol{\xi}'') + \frac{\Delta t^2}{8}\boldsymbol{\xi}'' - \frac{\Delta t^2}{24}\boldsymbol{\eta}''' - \frac{\Delta t}{2}\mathcal{J}(\boldsymbol{\sigma}(\boldsymbol{u}', p')\boldsymbol{n}) + \mathcal{O}(\Delta t^3) \quad \text{on } \Gamma \\
\rho_s h\boldsymbol{u}' + \mathcal{L}_s\boldsymbol{\eta} &= -\boldsymbol{\sigma}(\boldsymbol{u}, p)\boldsymbol{n} + \Delta t\boldsymbol{\sigma}(\boldsymbol{u}', p')\boldsymbol{n} - \rho_s h\mathcal{J}(\boldsymbol{\sigma}(\boldsymbol{u}', p')\boldsymbol{n} - \rho_s h\frac{\Delta t^2}{24}\boldsymbol{u}''' \\
&\quad - \frac{\Delta t^2}{8}\mathcal{L}_s\boldsymbol{\eta}'' - \frac{5}{8}\Delta t^2\boldsymbol{\sigma}(\boldsymbol{u}'', p'')\boldsymbol{n} + \mathcal{O}(\Delta t^3) \quad \text{on } \Gamma \\
\rho_f\boldsymbol{u}' - \nabla\cdot\boldsymbol{\sigma}(\boldsymbol{u}, p) &= -\frac{\Delta t^2}{24}\rho_f\boldsymbol{u}''' + \frac{\Delta t^2}{8}\nabla\cdot\boldsymbol{\sigma}(\boldsymbol{u}'', p'') + \mathcal{O}(\Delta t^4) \quad \text{in } \Omega \\
\boldsymbol{u} &= \boldsymbol{\xi} + \frac{\Delta t^2}{8}(\boldsymbol{u}'' - \boldsymbol{\xi}'') - \Delta t\mathcal{J}(\boldsymbol{\sigma}(\boldsymbol{u}', p')\boldsymbol{n}) + \mathcal{O}(\Delta t^3) \quad \text{on } \Gamma.
\end{aligned}$$

Next, using (4.8) in the first and fourth equations and noting that $\Delta t^2(\boldsymbol{u}'' - \boldsymbol{\xi}'') = \mathcal{O}(\Delta t^3)$, we get

$$\boldsymbol{\eta}' = \boldsymbol{\xi} + \frac{\Delta t^2}{8}\boldsymbol{\xi}'' - \frac{\Delta t^2}{24}\boldsymbol{\eta}''' - \frac{\Delta t}{2}\mathcal{J}(\boldsymbol{\sigma}(\boldsymbol{u}', p')\boldsymbol{n}) + \mathcal{O}(\Delta t^3) \quad \text{on } \Gamma \tag{4.9}$$

$$\begin{aligned}
\rho_s h\boldsymbol{u}' + \mathcal{L}_s\boldsymbol{\eta} &= -\boldsymbol{\sigma}(\boldsymbol{u}, p)\boldsymbol{n} + \Delta t\boldsymbol{\sigma}(\boldsymbol{u}', p')\boldsymbol{n} - \rho_s h\mathcal{J}(\boldsymbol{\sigma}(\boldsymbol{u}', p')\boldsymbol{n} \\
&\quad - \rho_s h\frac{\Delta t^2}{24}\boldsymbol{u}''' - \frac{\Delta t^2}{8}\mathcal{L}_s\boldsymbol{\eta}'' - \frac{5}{8}\Delta t^2\boldsymbol{\sigma}(\boldsymbol{u}'', p'')\boldsymbol{n} + \mathcal{O}(\Delta t^3) \quad \text{on } \Gamma
\end{aligned} \tag{4.10}$$

$$\rho_f\boldsymbol{u}' - \nabla\cdot\boldsymbol{\sigma}(\boldsymbol{u}, p) = -\frac{\Delta t^2}{24}\rho_f\boldsymbol{u}''' + \frac{\Delta t^2}{8}\nabla\cdot\boldsymbol{\sigma}(\boldsymbol{u}'', p'') + \mathcal{O}(\Delta t^4) \quad \text{in } \Omega \tag{4.11}$$

$$\boldsymbol{u} = \boldsymbol{\xi} - \Delta t\mathcal{J}(\boldsymbol{\sigma}(\boldsymbol{u}', p')\boldsymbol{n}) + \mathcal{O}(\Delta t^3) \quad \text{on } \Gamma. \tag{4.12}$$

Now we are going to rearrange the following expression from (4.6):

$$\boldsymbol{y} := \Delta t\boldsymbol{\sigma}(\boldsymbol{u}', p')\boldsymbol{n} - \rho_s h\mathcal{J}(\boldsymbol{\sigma}(\boldsymbol{u}', p')\boldsymbol{n}$$

as follows. Denote $\boldsymbol{x} := \boldsymbol{\sigma}(\boldsymbol{u}', p')\boldsymbol{n}$, then

$$\boldsymbol{y} = (\Delta t I - \rho_s h\mathcal{J})\boldsymbol{x}.$$

Using the definition of $\mathcal{J}$ (3.9), this is equivalent to $\frac{\Delta t}{\rho_s h}\boldsymbol{x} - \frac{1}{\rho_s h}\boldsymbol{y} = \mathcal{J}\boldsymbol{x}$, so

$$\begin{aligned}
\boldsymbol{x} &= \mathcal{J}^{-1}\Big(\frac{\Delta t}{\rho_s h}\boldsymbol{x} - \frac{1}{\rho_s h}\boldsymbol{y}\Big) = \Big(\frac{\rho_s h}{\Delta t}I + \frac{\Delta t}{4}\mathcal{L}_s\Big)\Big(\frac{\Delta t}{\rho_s h}\boldsymbol{x} - \frac{1}{\rho_s h}\boldsymbol{y}\Big) \\
&= \boldsymbol{x} - \frac{1}{\Delta t}\boldsymbol{y} + \frac{\Delta t^2}{4\rho_s h}\mathcal{L}_s\boldsymbol{x} - \frac{\Delta t}{4\rho_s h}\mathcal{L}_s\boldsymbol{y}
\end{aligned}$$

or equivalently,

$$\frac{1}{\Delta t}\boldsymbol{y} + \frac{\Delta t}{4\rho_s h}\mathcal{L}_s\boldsymbol{y} = \frac{\Delta t^2}{4\rho_s h}\mathcal{L}_s\boldsymbol{x}.$$

Using further manipulations, we have

$$\begin{aligned}\Big(\frac{\rho_s h}{\Delta t}I+\frac{\Delta t}{4}\mathcal{L}_s\Big)\boldsymbol{y} &= \frac{\Delta t^2}{4}\mathcal{L}_s\boldsymbol{x}\\ \mathcal{J}^{-1}\boldsymbol{y} &= \frac{\Delta t^2}{4}\mathcal{L}_s\boldsymbol{x}\\ \boldsymbol{y} &= \frac{\Delta t^2}{4}\mathcal{J}\mathcal{L}_s\boldsymbol{x}\end{aligned}$$

so

$$\Delta t\boldsymbol{\sigma}(\boldsymbol{u}',p')\boldsymbol{n}-\rho_s h\mathcal{J}(\boldsymbol{\sigma}(\boldsymbol{u}',p')\boldsymbol{n}=\frac{\Delta t^2}{4}\mathcal{J}\mathcal{L}_s\boldsymbol{\sigma}(\boldsymbol{u}',p')\boldsymbol{n}.$$

Using the relation above, equation (4.6) can be written as

$$\begin{aligned}\rho_s h\boldsymbol{u}'+\mathcal{L}_s\boldsymbol{\eta} &= -\boldsymbol{\sigma}(\boldsymbol{u},p)\boldsymbol{n}+\frac{\Delta t^2}{4}\mathcal{J}\mathcal{L}_s\boldsymbol{\sigma}(\boldsymbol{u}',p')\boldsymbol{n}-\rho_s h\frac{\Delta t^2}{24}\boldsymbol{u}'''\\ &\quad-\frac{\Delta t^2}{8}\mathcal{L}_s\boldsymbol{\eta}''-\frac{5}{8}\Delta t^2\boldsymbol{\sigma}(\boldsymbol{u}'',p'')\boldsymbol{n}+\mathcal{O}(\Delta t^3)\quad\text{on }\Gamma.\end{aligned}$$

Using the first derivative of (4.12), we can write

$$\begin{aligned}\rho_s h\Big(\boldsymbol{\xi}'-\Delta t\mathcal{J}(\boldsymbol{\sigma}(\boldsymbol{u}'',p'')\boldsymbol{n})\Big)+\mathcal{L}_s\boldsymbol{\eta} &= -\boldsymbol{\sigma}(\boldsymbol{u},p)\boldsymbol{n}+\frac{\Delta t^2}{4}\mathcal{J}\mathcal{L}_s\boldsymbol{\sigma}(\boldsymbol{u}',p')\boldsymbol{n}\\ &\quad-\rho_s h\frac{\Delta t^2}{24}\boldsymbol{u}'''-\frac{\Delta t^2}{8}\mathcal{L}_s\boldsymbol{\eta}''-\frac{5}{8}\Delta t^2\boldsymbol{\sigma}(\boldsymbol{u}'',p'')\boldsymbol{n}+\mathcal{O}(\Delta t^3)\quad\text{on }\Gamma.\end{aligned}$$

Rearranging and use the bound (3.10), we have

$$\begin{aligned}\rho_s h\boldsymbol{\xi}'+\mathcal{L}_s\boldsymbol{\eta} &= -\boldsymbol{\sigma}(\boldsymbol{u},p)\boldsymbol{n}+\Delta t\rho_s h\mathcal{J}(\boldsymbol{\sigma}(\boldsymbol{u}'',p'')\boldsymbol{n})\\ &\quad-\rho_s h\frac{\Delta t^2}{24}\boldsymbol{u}'''-\frac{\Delta t^2}{8}\mathcal{L}_s\boldsymbol{\eta}''-\frac{5}{8}\Delta t^2\boldsymbol{\sigma}(\boldsymbol{u}'',p'')\boldsymbol{n}+\mathcal{O}(\Delta t^3)\quad\text{on }\Gamma.\end{aligned}$$

Finally, the local truncation error is given by

$$\begin{aligned}\boldsymbol{\eta}' &= \boldsymbol{\xi}+\frac{\Delta t^2}{8}\boldsymbol{\xi}''-\frac{\Delta t^2}{24}\boldsymbol{\eta}'''-\frac{\Delta t}{2}\mathcal{J}(\boldsymbol{\sigma}(\boldsymbol{u}',p')\boldsymbol{n})+\mathcal{O}(\Delta t^3)\quad\text{on }\Gamma\\ \rho_s h\boldsymbol{\xi}'+\mathcal{L}_s\boldsymbol{\eta} &= -\boldsymbol{\sigma}(\boldsymbol{u},p)\boldsymbol{n}+\Delta t\rho_s h\mathcal{J}(\boldsymbol{\sigma}(\boldsymbol{u}'',p'')\boldsymbol{n})\\ &\quad-\rho_s h\frac{\Delta t^2}{24}\boldsymbol{u}'''-\frac{\Delta t^2}{8}\mathcal{L}_s\boldsymbol{\eta}''-\frac{5}{8}\Delta t^2\boldsymbol{\sigma}(\boldsymbol{u}'',p'')\boldsymbol{n}+\mathcal{O}(\Delta t^3)\quad\text{on }\Gamma\\ \rho_f\boldsymbol{u}'-\nabla\cdot\boldsymbol{\sigma}(\boldsymbol{u},p) &= -\frac{\Delta t^2}{24}\rho_f\boldsymbol{u}'''+\frac{\Delta t^2}{8}\nabla\cdot\boldsymbol{\sigma}(\boldsymbol{u}'',p'')+\mathcal{O}(\Delta t^4)\quad\text{in }\Omega\\ \nabla\cdot\boldsymbol{u} &= \mathcal{O}(\Delta t^3)\quad\text{in }\Omega\\ \boldsymbol{u} &= \boldsymbol{\xi}-\Delta t\mathcal{J}(\boldsymbol{\sigma}(\boldsymbol{u}',p')\boldsymbol{n})+\mathcal{O}(\Delta t^3)\quad\text{on }\Gamma.\end{aligned}$$

Similar to before, in the following, when there is no confusion, we will assume that the functions typeset without a time argument are evaluated at t. Denoting the displacement by $\boldsymbol{d}$, the structure velocity by $\boldsymbol{w}$, the fluid velocity by $\boldsymbol{v}$, and the fluid pressure by q, method (3.5)–(3.8) is therefore consistent of $\mathcal{O}(\Delta t^3)$ with the following modified equations (see, e.g., [18, 26, 27, 34, 36, 44]):

$$\boldsymbol{d}' = \boldsymbol{w}+\frac{\Delta t^2}{8}\boldsymbol{w}''-\frac{\Delta t^2}{24}\boldsymbol{d}'''-\frac{\Delta t}{2}\mathcal{J}(\boldsymbol{\sigma}(\boldsymbol{v}',q')\boldsymbol{n})\quad\text{on }\Gamma \tag{4.13}$$

$$\begin{aligned}\rho_s h\boldsymbol{w}'+\mathcal{L}_s\boldsymbol{d} &= -\boldsymbol{\sigma}(\boldsymbol{v},q)\boldsymbol{n}+\Delta t\rho_s h\mathcal{J}(\boldsymbol{\sigma}(\boldsymbol{v}'',q'')\boldsymbol{n})-\rho_s h\frac{\Delta t^2}{24}\boldsymbol{v}'''\\ &\quad-\frac{\Delta t^2}{8}\mathcal{L}_s\boldsymbol{d}''-\frac{5}{8}\Delta t^2\boldsymbol{\sigma}(\boldsymbol{v}'',q'')\boldsymbol{n}\quad\text{on }\Gamma\end{aligned} \tag{4.14}$$

$$\rho_f\boldsymbol{v}'-\nabla\cdot\boldsymbol{\sigma}(\boldsymbol{v},q) = -\frac{\Delta t^2}{24}\rho_f\boldsymbol{v}'''+\frac{\Delta t^2}{8}\nabla\cdot\boldsymbol{\sigma}(\boldsymbol{v}'',q'')\quad\text{in }\Omega \tag{4.15}$$

$$\nabla\cdot\boldsymbol{v} = 0\quad\text{in }\Omega \tag{4.16}$$

$$\boldsymbol{v} = \boldsymbol{w}-\Delta t\mathcal{J}(\boldsymbol{\sigma}(\boldsymbol{v}',q')\boldsymbol{n})\quad\text{on }\Gamma \tag{4.17}$$

where we assume that the 'modified' variables $\boldsymbol{d}$, $\boldsymbol{w}$, $\boldsymbol{v}$, and q are smooth enough for the quantities involved to be well-defined. The differences in the structure displacement, structure velocity, fluid velocity, and pressure $\boldsymbol{d}-\boldsymbol{\eta}$, $\boldsymbol{w}-\boldsymbol{\xi}$, $\boldsymbol{v}-\boldsymbol{u}$, and $q-p$, respectively, satisfy the following partial differential system

$$(\boldsymbol{d}-\boldsymbol{\eta})' = (\boldsymbol{w}-\boldsymbol{\xi}) + \frac{\Delta t^2}{8}\boldsymbol{w}'' - \frac{\Delta t^2}{24}\boldsymbol{d}''' - \frac{\Delta t}{2}\mathcal{J}(\boldsymbol{\sigma}(\boldsymbol{v}', q')\boldsymbol{n}) \quad \text{on } \Gamma \tag{4.18}$$

$$\begin{aligned}\rho_s h(\boldsymbol{w}-\boldsymbol{\xi})' + \mathcal{L}_s(\boldsymbol{d}-\boldsymbol{\eta}) = & -\boldsymbol{\sigma}(\boldsymbol{v}-\boldsymbol{u}, q-p)\boldsymbol{n} + \Delta t\rho_s h\mathcal{J}(\boldsymbol{\sigma}(\boldsymbol{v}'', q'')\boldsymbol{n}) \\ & - \rho_s h\frac{\Delta t^2}{24}\boldsymbol{v}''' - \frac{\Delta t^2}{8}\mathcal{L}_s\boldsymbol{d}'' - \frac{5}{8}\Delta t^2\boldsymbol{\sigma}(\boldsymbol{v}'', q'')\boldsymbol{n} \quad \text{on } \Gamma\end{aligned} \tag{4.19}$$

$$\rho_f(\boldsymbol{v}-\boldsymbol{u})' - \nabla\cdot\boldsymbol{\sigma}(\boldsymbol{v}-\boldsymbol{u}, q-p) = -\frac{\Delta t^2}{24}\rho_f\boldsymbol{v}''' + \frac{\Delta t^2}{8}\nabla\cdot\boldsymbol{\sigma}(\boldsymbol{v}'', q'') \quad \text{in } \Omega \tag{4.20}$$

$$\nabla\cdot(\boldsymbol{v}-\boldsymbol{u}) = 0 \quad \text{in } \Omega \tag{4.21}$$

$$\boldsymbol{v}-\boldsymbol{u} = \boldsymbol{w}-\boldsymbol{\xi} - \Delta t\mathcal{J}(\boldsymbol{\sigma}(\boldsymbol{v}', q')\boldsymbol{n}) \quad \text{on } \Gamma. \tag{4.22}$$

We will now use the standard energy estimates to show that $\boldsymbol{d}$, $\boldsymbol{w}$, $\boldsymbol{v}$, q generate a manifold $\mathcal{O}(\Delta t^2)$-close to the $\boldsymbol{\eta}$, $\boldsymbol{\xi}$, $\boldsymbol{u}$, p solution manifold. First, we introduce the following notation. Let $\mathcal{E}_e$ denote the sum of the kinetic and elastic energy and $\mathcal{D}_e$ denote the dissipation, given by

$$\begin{aligned}\mathcal{E}_e &= \frac{1}{2}\|\boldsymbol{d}-\boldsymbol{\eta}\|_S^2 + \frac{\rho_s h}{4}\|\boldsymbol{w}-\boldsymbol{\xi}\|_{L^2(\Gamma)}^2 + \frac{\rho_f}{2}\|\boldsymbol{v}-\boldsymbol{u}\|_{L^2(\Omega)}^2 \\ \mathcal{D}_e &= 2\mu\|\boldsymbol{D}(\boldsymbol{v}-\boldsymbol{u})\|_{L^2(\Omega)}^2.\end{aligned}$$

The main results of this section is given in the following theorem.

Theorem 4.1. *Assume that the solution $\boldsymbol{\eta}$, $\boldsymbol{\xi}$, $\boldsymbol{u}$, p of* (3.1)–(3.4) *satisfies the regularity assumptions in Hypothesis* 4.1*, and that the system is isolated, i.e., $p_{\text{in}} = p_{\text{out}} = 0$. Then, the following estimate holds*

$$\mathcal{E}_e(t) + \int_0^t \mathcal{D}_e(\tau)\,\mathrm{d}\tau \leqslant \Delta t^4 \mathrm{e}^t\left(\int_0^t \mathcal{O}_1(\tau)\,\mathrm{d}\tau + \mathcal{O}_2(t)\right)$$

where

$$\begin{aligned}\mathcal{O}_1 = & \frac{1}{2}\Big(\frac{1}{8}\|\boldsymbol{w}''\|_S + \frac{1}{24}\|\boldsymbol{d}'''\|_S + \frac{3}{2}\frac{C_{P,S}}{\rho_s h}\|\mathcal{L}_s(\boldsymbol{\sigma}(\boldsymbol{v}', q')\boldsymbol{n})\|_{L^2(\Gamma)}\Big)^2 \\ & + \frac{1}{\rho_s h}\Big(\frac{1}{8}\|\mathcal{L}_s\boldsymbol{d}''\|_{L^2(\Gamma)} + \frac{5}{8}\|(\boldsymbol{\sigma}(\boldsymbol{v}'', q'')\boldsymbol{n}\|_{L^2(\Gamma)} + \frac{\rho_s h}{24}\|\boldsymbol{v}'''\|_{L^2(\Gamma)}\Big)^2 \\ & + \frac{1}{1152\rho_f}\Big(\rho_f\|\boldsymbol{v}'''\|_{L^2(\Omega)} + 3\|\nabla\cdot\boldsymbol{\sigma}(\boldsymbol{v}'', q'')\|_{L^2(\Omega)}\Big)^2 + \frac{1}{2\rho_s h}\|\boldsymbol{\sigma}(\boldsymbol{v}', q')\boldsymbol{n}\|_{L^2(\Gamma)}^2 \\ & + \frac{1}{2\rho_s h}\Big(\|\boldsymbol{\sigma}(\boldsymbol{v}'', q'')\boldsymbol{n}\|_{L^2(\Gamma)} + \frac{\rho_s h}{24}\|\boldsymbol{v}'''\|_{L^2(\Gamma)} + \frac{1}{64}\|\mathcal{L}_s\boldsymbol{d}''\|_{L^2(\Gamma)} + \frac{5}{8}\|\boldsymbol{\sigma}(\boldsymbol{v}'', q'')\boldsymbol{n}\|_{L^2(\Gamma)}\Big)^2 \\ \mathcal{O}_2 = & \frac{1}{\rho_s h}\|\boldsymbol{\sigma}(\boldsymbol{v}', q')\boldsymbol{n}\|_{L^2(\Gamma)}^2 + \frac{1}{\rho_s h}\|\boldsymbol{\sigma}(\boldsymbol{v}'(0), q'(0))\boldsymbol{n}\|_{L^2(\Gamma)}^2.\end{aligned}$$

Proof. We multiply (4.18) by $\mathcal{L}_s(\boldsymbol{d}-\boldsymbol{\eta})$, (4.19) by $\boldsymbol{w}-\boldsymbol{\xi}$, (4.20) by $\boldsymbol{v}-\boldsymbol{u}$, and (4.21) by $q-p$, then add, integrate by parts on Γ (assuming that $\boldsymbol{w}'' = \boldsymbol{d}''' = \mathcal{J}(\boldsymbol{\sigma}(\boldsymbol{v}', q')\boldsymbol{n})\cdot\boldsymbol{n} = 0$ on $\partial\Gamma$), and use (4.22) as follows

$$\begin{aligned}&\frac{1}{2}\frac{\mathrm{d}}{\mathrm{d}t}\|\boldsymbol{d}-\boldsymbol{\eta}\|_S^2 + \frac{\rho_s h}{2}\frac{\mathrm{d}}{\mathrm{d}t}\|\boldsymbol{w}-\boldsymbol{\xi}\|_{L^2(\Gamma)}^2 + \frac{\rho_f}{2}\frac{\mathrm{d}}{\mathrm{d}t}\|\boldsymbol{v}-\boldsymbol{u}\|_{L^2(\Omega)}^2 + 2\mu\|\boldsymbol{D}(\boldsymbol{v}-\boldsymbol{u})\|_{L^2(\Omega)}^2 \\ &\quad = \frac{\Delta t^2}{8}\int_\Gamma \boldsymbol{w}''\mathcal{L}_s(\boldsymbol{d}-\boldsymbol{\eta}) - \frac{\Delta t^2}{24}\int_\Gamma \boldsymbol{d}'''\mathcal{L}_s(\boldsymbol{d}-\boldsymbol{\eta}) - \frac{\Delta t}{2}\int_\Gamma \mathcal{J}(\boldsymbol{\sigma}(\boldsymbol{v}', q')\boldsymbol{n})\mathcal{L}_s(\boldsymbol{d}-\boldsymbol{\eta}) \\ &\qquad + \Delta t\rho_s h\int_\Gamma \mathcal{J}(\boldsymbol{\sigma}(\boldsymbol{v}'', q'')\boldsymbol{n})(\boldsymbol{w}-\boldsymbol{\xi}) - \rho_s h\frac{\Delta t^2}{24}\int_\Gamma \boldsymbol{v}'''(\boldsymbol{w}-\boldsymbol{\xi}) \\ &\qquad - \frac{\Delta t^2}{8}\int_\Gamma \mathcal{L}_s\boldsymbol{d}''(\boldsymbol{w}-\boldsymbol{\xi}) - \frac{5}{8}\Delta t^2\int_\Gamma \boldsymbol{\sigma}(\boldsymbol{v}'', q'')\boldsymbol{n}\,(\boldsymbol{w}-\boldsymbol{\xi}) - \frac{\Delta t^2}{24}\rho_f\int_\Omega \boldsymbol{v}'''(\boldsymbol{v}-\boldsymbol{u}) \\ &\qquad - \Delta t\int_\Gamma \boldsymbol{\sigma}(\boldsymbol{v}-\boldsymbol{u}, q-p)\boldsymbol{n}\,\mathcal{J}(\boldsymbol{\sigma}(\boldsymbol{v}', q')\boldsymbol{n}) + \frac{\Delta t^2}{8}\int_\Omega \nabla\cdot\boldsymbol{\sigma}(\boldsymbol{v}'', q'')(\boldsymbol{v}-\boldsymbol{u}).\end{aligned}$$

Using (4.19), we have

$$
\begin{aligned}
-\int_\Gamma \boldsymbol{\sigma}(\boldsymbol{v}-\boldsymbol{u}, q-p)\boldsymbol{n}\mathcal{J}(\boldsymbol{\sigma}(\boldsymbol{v}', q')\boldsymbol{n}) &= \rho_s h\int_\Gamma (\boldsymbol{w}-\boldsymbol{\xi})'\mathcal{J}(\boldsymbol{\sigma}(\boldsymbol{v}', q')\boldsymbol{n}) + \int_\Gamma \mathcal{L}_s(\boldsymbol{d}-\boldsymbol{\eta})\mathcal{J}(\boldsymbol{\sigma}(\boldsymbol{v}', q')\boldsymbol{n}) \\
&\quad - \rho_s h\Delta t\int_\Gamma \mathcal{J}(\boldsymbol{\sigma}(\boldsymbol{v}'', q'')\boldsymbol{n}\mathcal{J}(\boldsymbol{\sigma}(\boldsymbol{v}', q')\boldsymbol{n}) + \rho_s h\frac{\Delta t^2}{24}\int_\Gamma \boldsymbol{v}'''\mathcal{J}(\boldsymbol{\sigma}(\boldsymbol{v}', q')\boldsymbol{n}) \\
&\quad + \frac{\Delta t^2}{8}\int_\Gamma \mathcal{L}_s\boldsymbol{d}''\mathcal{J}(\boldsymbol{\sigma}(\boldsymbol{v}', q')\boldsymbol{n}) + \frac{5}{8}\Delta t^2\int_\Gamma \boldsymbol{\sigma}(\boldsymbol{v}'', q'')\boldsymbol{n}\mathcal{J}(\boldsymbol{\sigma}(\boldsymbol{v}', q')\boldsymbol{n}).
\end{aligned}
$$

Using the relation above, the Cauchy–Schwarz inequality, symmetry of operator $\mathcal{L}_s$, the Poincaré inequality, and the bound (3.10) we have

$$
\begin{aligned}
&\frac{1}{2}\frac{\mathrm{d}}{\mathrm{d}t}\|\boldsymbol{d}-\boldsymbol{\eta}\|_S^2 + \frac{\rho_s h}{2}\frac{\mathrm{d}}{\mathrm{d}t}\|\boldsymbol{w}-\boldsymbol{\xi}\|_{L^2(\Gamma)}^2 + \frac{\rho_f}{2}\frac{\mathrm{d}}{\mathrm{d}t}\|\boldsymbol{v}-\boldsymbol{u}\|_{L^2(\Omega)}^2 + 2\mu\|\boldsymbol{D}(\boldsymbol{v}-\boldsymbol{u})\|_{L^2(\Omega)}^2 \\
&\quad\leqslant \frac{\Delta t^2}{8}\|\boldsymbol{w}''\|_S\|\boldsymbol{d}-\boldsymbol{\eta}\|_S + \frac{\Delta t^2}{24}\|\boldsymbol{d}'''\|_S\|\boldsymbol{d}-\boldsymbol{\eta}\|_S \\
&\qquad + \frac{\Delta t}{2}\|\mathcal{L}_s\mathcal{J}(\boldsymbol{\sigma}(\boldsymbol{v}', q')\boldsymbol{n})\|_{L^2(\Gamma)}\|\boldsymbol{d}-\boldsymbol{\eta}\|_{L^2(\Gamma)} + \Delta t\rho_s h\int_\Gamma \mathcal{J}(\boldsymbol{\sigma}(\boldsymbol{v}'', q'')\boldsymbol{n})(\boldsymbol{w}-\boldsymbol{\xi}) \\
&\qquad + \rho_s h\frac{\Delta t^2}{24}\|\boldsymbol{v}'''\|_{L^2(\Gamma)}\|\boldsymbol{w}-\boldsymbol{\xi}\|_{L^2(\Gamma)} + \frac{\Delta t^2}{8}\|\mathcal{L}_s\boldsymbol{d}''\|_{L^2(\Gamma)}\|\boldsymbol{w}-\boldsymbol{\xi}\|_{L^2(\Gamma)} \\
&\qquad + \frac{5}{8}\Delta t^2\|\boldsymbol{\sigma}(\boldsymbol{v}'', q'')\boldsymbol{n}\|_{L^2(\Gamma)}\|\boldsymbol{w}-\boldsymbol{\xi}\|_{L^2(\Gamma)} + \rho_s h\Delta t\int_\Gamma (\boldsymbol{w}-\boldsymbol{\xi})'\mathcal{J}(\boldsymbol{\sigma}(\boldsymbol{v}', q')\boldsymbol{n}) \\
&\qquad + \Delta t\|\boldsymbol{d}-\boldsymbol{\eta}\|_{L^2(\Gamma)}\|\mathcal{L}_s\mathcal{J}(\boldsymbol{\sigma}(\boldsymbol{v}', q')\boldsymbol{n})\|_{L^2(\Gamma)} \\
&\qquad + \rho_s h\Delta t^2\|\mathcal{J}(\boldsymbol{\sigma}(\boldsymbol{v}'', q'')\boldsymbol{n})\|_{L^2(\Gamma)}\|\mathcal{J}(\boldsymbol{\sigma}(\boldsymbol{v}', q')\boldsymbol{n})\|_{L^2(\Gamma)} \\
&\qquad + \rho_s h\frac{\Delta t^3}{24}\|\boldsymbol{v}'''\|_{L^2(\Gamma)}\|\mathcal{J}(\boldsymbol{\sigma}(\boldsymbol{v}', q')\boldsymbol{n})\|_{L^2(\Gamma)} + \frac{\Delta t^3}{8}\|\mathcal{L}_s\boldsymbol{d}''\|_{L^2(\Gamma)}\|\mathcal{J}(\boldsymbol{\sigma}(\boldsymbol{v}', q')\boldsymbol{n})\|_{L^2(\Gamma)} \\
&\qquad + \frac{5}{8}\Delta t^3\|\boldsymbol{\sigma}(\boldsymbol{v}'', q'')\boldsymbol{n}\|_{L^2(\Gamma)}\|\mathcal{J}(\boldsymbol{\sigma}(\boldsymbol{v}', q')\boldsymbol{n})\|_{L^2(\Gamma)} + \frac{\Delta t^2}{24}\rho_f\|\boldsymbol{v}'''\|_{L^2(\Omega)}\|\boldsymbol{v}-\boldsymbol{u}\|_{L^2(\Omega)} \\
&\qquad + \frac{\Delta t^2}{8}\|\nabla\cdot\boldsymbol{\sigma}(\boldsymbol{v}'', q'')\|_{L^2(\Omega)}\|\boldsymbol{v}-\boldsymbol{u}\|_{L^2(\Omega)}.
\end{aligned}
$$

Applying (2.9) and (3.10) and grouping similar terms together, we obtain

$$
\begin{aligned}
&\frac{1}{2}\frac{\mathrm{d}}{\mathrm{d}t}\|\boldsymbol{d}-\boldsymbol{\eta}\|_S^2 + \frac{\rho_s h}{2}\frac{\mathrm{d}}{\mathrm{d}t}\|\boldsymbol{w}-\boldsymbol{\xi}\|_{L^2(\Gamma)}^2 + \frac{\rho_f}{2}\frac{\mathrm{d}}{\mathrm{d}t}\|\boldsymbol{v}-\boldsymbol{u}\|_{L^2(\Omega)}^2 + 2\mu\|\boldsymbol{D}(\boldsymbol{v}-\boldsymbol{u})\|_{L^2(\Omega)}^2 \\
&\quad\leqslant \Delta t^2\Big(\frac{1}{8}\|\boldsymbol{w}''\|_S + \frac{1}{24}\|\boldsymbol{d}'''\|_S + \frac{3}{2}\frac{C_{P,S}}{\rho_s h}\|\mathcal{L}_s(\boldsymbol{\sigma}(\boldsymbol{v}', q')\boldsymbol{n})\|_{L^2(\Gamma)}\Big)\|\boldsymbol{d}-\boldsymbol{\eta}\|_S \\
&\qquad + \Delta t^2\Big(\frac{1}{8}\|\mathcal{L}_s\boldsymbol{d}''\|_{L^2(\Gamma)} + \frac{5}{8}\|\boldsymbol{\sigma}(\boldsymbol{v}'', q'')\boldsymbol{n}\|_{L^2(\Gamma)} + \frac{\rho_s h}{24}\|\boldsymbol{v}'''\|_{L^2(\Gamma)}\Big)\|\boldsymbol{w}-\boldsymbol{\xi}\|_{L^2(\Gamma)} \\
&\qquad + \frac{\Delta t^2}{24}\Big(\rho_f\|\boldsymbol{v}'''\|_{L^2(\Omega)} + 3\|\nabla\cdot\boldsymbol{\sigma}(\boldsymbol{v}'', q'')\|_{L^2(\Omega)}\Big)\|\boldsymbol{v}-\boldsymbol{u}\|_{L^2(\Omega)} \\
&\qquad + \frac{\Delta t^4}{\rho_s h}\Big(\|\boldsymbol{\sigma}(\boldsymbol{v}'', q'')\boldsymbol{n}\|_{L^2(\Gamma)} + \frac{\rho_s h}{24}\|\boldsymbol{v}'''\|_{L^2(\Gamma)} + \frac{5}{8}\|\boldsymbol{\sigma}(\boldsymbol{v}'', q'')\boldsymbol{n}\|_{L^2(\Gamma)}\Big) \\
&\qquad + \frac{\Delta t^4}{8\rho_s h}\|\mathcal{L}_s\boldsymbol{d}''\|_{L^2(\Gamma)}\|\boldsymbol{\sigma}(\boldsymbol{v}', q')\boldsymbol{n}\|_{L^2(\Gamma)} + \Delta t\rho_s h\int_\Gamma \mathcal{J}(\boldsymbol{\sigma}(\boldsymbol{v}'', q'')\boldsymbol{n})(\boldsymbol{w}-\boldsymbol{\xi}) \\
&\qquad + \Delta t\rho_s h\int_\Gamma (\boldsymbol{w}-\boldsymbol{\xi})'\mathcal{J}(\boldsymbol{\sigma}(\boldsymbol{v}', q')\boldsymbol{n}).
\end{aligned}
$$

Using Young's inequality, we have

$$\begin{aligned}
&\frac{\mathrm{d}}{\mathrm{d}t}\Big(\frac{1}{2}\|\boldsymbol{d}-\boldsymbol{\eta}\|_S^2+\frac{\rho_s h}{2}\|\boldsymbol{w}-\boldsymbol{\xi}\|_{L^2(\Gamma)}^2+\frac{\rho_f}{2}\|\boldsymbol{v}-\boldsymbol{u}\|_{L^2(\Omega)}^2\Big)+2\mu\|\boldsymbol{D}(\boldsymbol{v}-\boldsymbol{u})\|_{L^2(\Omega)}^2\\
&\quad\leqslant\frac{1}{2}\|\boldsymbol{d}-\boldsymbol{\eta}\|_S^2+\frac{\rho_s h}{4}\|\boldsymbol{w}-\boldsymbol{\xi}\|_{L^2(\Gamma)}^2+\frac{\rho_f}{2}\|\boldsymbol{v}-\boldsymbol{u}\|_{L^2(\Omega)}^2+\frac{\Delta t^4}{2\rho_s h}\|\boldsymbol{\sigma}(\boldsymbol{v}',q')\boldsymbol{n}\|_{L^2(\Gamma)}^2\\
&\qquad+\frac{\Delta t^4}{2}\Big(\frac{1}{8}\|\boldsymbol{w}''\|_S+\frac{1}{24}\|\boldsymbol{d}'''\|_S+\frac{3}{2}\frac{C_{P,S}}{\rho_s h}\|\mathcal{L}_s(\boldsymbol{\sigma}(\boldsymbol{v}',q')\boldsymbol{n})\|_{L^2(\Gamma)}\Big)^2\\
&\qquad+\frac{\Delta t^4}{\rho_s h}\Big(\frac{1}{8}\|\mathcal{L}_s\boldsymbol{d}''\|_{L^2(\Gamma)}+\frac{5}{8}\|\boldsymbol{\sigma}(\boldsymbol{v}'',q'')\boldsymbol{n}\|_{L^2(\Gamma)}+\frac{\rho_s h}{24}\|\boldsymbol{v}'''\|_{L^2(\Gamma)}\Big)^2\\
&\qquad+\frac{\Delta t^4}{1152\rho_f}\Big(\rho_f\|\boldsymbol{v}'''\|_{L^2(\Omega)}+3\|\nabla\cdot\boldsymbol{\sigma}(\boldsymbol{v}'',q'')\|_{L^2(\Omega)}\Big)^2\\
&\qquad+\frac{\Delta t^4}{2\rho_s h}\Big(\|\boldsymbol{\sigma}(\boldsymbol{v}'',q'')\boldsymbol{n}\|_{L^2(\Gamma)}+\frac{\rho_s h}{24}\|\boldsymbol{v}'''\|_{L^2(\Gamma)}+\frac{1}{64}\|\mathcal{L}_s\boldsymbol{d}''\|_{L^2(\Gamma)}\\
&\qquad+\frac{5}{8}\|\boldsymbol{\sigma}(\boldsymbol{v}'',q'')\boldsymbol{n}\|_{L^2(\Gamma)}\Big)^2\\
&\qquad+\Delta t\rho_s h\int_\Gamma\mathcal{J}(\boldsymbol{\sigma}(\boldsymbol{v}'',q'')\boldsymbol{n})(\boldsymbol{w}-\boldsymbol{\xi})+\Delta t\rho_s h\int_\Gamma(\boldsymbol{w}-\boldsymbol{\xi})'\mathcal{J}(\boldsymbol{\sigma}(\boldsymbol{v}',q')\boldsymbol{n}).
\end{aligned}$$

Integrating from 0 to t and integrating the last integral by parts in time, we have

$$\begin{aligned}
&\frac{1}{2}\|\boldsymbol{d}(t)-\boldsymbol{\eta}(t)\|_S^2+\frac{\rho_s h}{2}\|\boldsymbol{w}(t)-\boldsymbol{\xi}(t)\|_{L^2(\Gamma)}^2+\frac{\rho_f}{2}\|\boldsymbol{v}(t)-\boldsymbol{u}(t)\|_{L^2(\Omega)}^2+2\mu\int_0^t\|\boldsymbol{D}(\boldsymbol{v}(\tau)-\boldsymbol{u}(\tau))\|_{L^2(\Omega)}^2\,\mathrm{d}\tau\\
&\quad\leqslant\frac{1}{2}\|\boldsymbol{d}(0)-\boldsymbol{\eta}(0)\|_S^2+\frac{\rho_s h}{2}\|\boldsymbol{w}(0)-\boldsymbol{\xi}(0)\|_{L^2(\Gamma)}^2+\frac{\rho_f}{2}\|\boldsymbol{v}(0)-\boldsymbol{u}(0)\|_{L^2(\Omega)}^2\\
&\qquad+\int_0^t\Big(\frac{1}{2}\|\boldsymbol{d}(\tau)-\boldsymbol{\eta}(\tau)\|_S^2+\frac{\rho_s h}{4}\|\boldsymbol{w}(\tau)-\boldsymbol{\xi}(\tau)\|_{L^2(\Gamma)}^2+\frac{\rho_f}{2}\|\boldsymbol{v}(\tau)-\boldsymbol{u}(\tau)\|_{L^2(\Omega)}^2\Big)\,\mathrm{d}\tau\\
&\qquad+\frac{\Delta t^4}{2}\int_0^t\Big(\frac{1}{8}\|\boldsymbol{w}''(\tau)\|_S+\frac{1}{24}\|\boldsymbol{d}'''(\tau)\|_S+\frac{3}{2}\frac{C_{P,S}}{\rho_s h}\|\mathcal{L}_s(\boldsymbol{\sigma}(\boldsymbol{v}'(\tau),q'(\tau))\boldsymbol{n})\|_{L^2(\Gamma)}\Big)^2\,\mathrm{d}\tau\\
&\qquad+\frac{\Delta t^4}{\rho_s h}\int_0^t\Big(\frac{1}{8}\|\mathcal{L}_s\boldsymbol{d}''(\tau)\|_{L^2(\Gamma)}+\frac{5}{8}\|\boldsymbol{\sigma}(\boldsymbol{v}''(\tau),q''(\tau))\boldsymbol{n}\|_{L^2(\Gamma)}+\frac{\rho_s h}{24}\|\boldsymbol{v}'''(\tau)\|_{L^2(\Gamma)}\Big)^2\,\mathrm{d}\tau\\
&\qquad+\frac{\Delta t^4}{1152\rho_f}\int_0^t\Big(\rho_f\|\boldsymbol{v}'''(\tau)\|_{L^2(\Omega)}+3\|\nabla\cdot\boldsymbol{\sigma}(\boldsymbol{v}''(\tau),q''(\tau))\|_{L^2(\Omega)}\Big)^2\,\mathrm{d}\tau\\
&\qquad+\frac{\Delta t^4}{2\rho_s h}\int_0^t\|\boldsymbol{\sigma}(\boldsymbol{v}'(\tau),q'(\tau))\boldsymbol{n}\|_{L^2(\Gamma)}^2\,\mathrm{d}\tau\\
&\qquad+\frac{\Delta t^4}{2\rho_s h}\int_0^t\Big(\|\boldsymbol{\sigma}(\boldsymbol{v}''(\tau),q''(\tau))\boldsymbol{n}\|_{L^2(\Gamma)}+\frac{\rho_s h}{24}\|\boldsymbol{v}'''(\tau)\|_{L^2(\Gamma)}+\frac{1}{64}\|\mathcal{L}_s\boldsymbol{d}''(\tau)\|_{L^2(\Gamma)}\\
&\qquad+\frac{5}{8}\|\boldsymbol{\sigma}(\boldsymbol{v}''(\tau),q''(\tau))\boldsymbol{n}\|_{L^2(\Gamma)}\Big)^2\,\mathrm{d}\tau+\Delta t\rho_s h\int_\Gamma(\boldsymbol{w}(t)-\boldsymbol{\xi}(t))\mathcal{J}(\boldsymbol{\sigma}(\boldsymbol{v}'(t),q'(t))\boldsymbol{n})\\
&\qquad-\Delta t\rho_s h\int_\Gamma(\boldsymbol{w}(0)-\boldsymbol{\xi}(0))\mathcal{J}(\boldsymbol{\sigma}(\boldsymbol{v}'(0),q'(0))\boldsymbol{n}).
\end{aligned}$$

We apply the Cauchy–Schwarz and Young's inequalities to last couple of terms as follows

$$\begin{aligned}
&\Delta t\rho_s h\int_\Gamma(\boldsymbol{w}(t)-\boldsymbol{\xi}(t))\mathcal{J}(\boldsymbol{\sigma}(\boldsymbol{v}'(t),q'(t))\boldsymbol{n})-\Delta t\rho_s h\int_\Gamma(\boldsymbol{w}(0)-\boldsymbol{\xi}(0))\mathcal{J}(\boldsymbol{\sigma}(\boldsymbol{v}'(0),q'(0))\boldsymbol{n})\\
&\quad\leqslant\frac{\rho^s h}{4}\|\boldsymbol{w}(t)-\boldsymbol{\xi}(t)\|_{L^2(\Gamma)}^2+\Delta t^2\rho^s h\|\mathcal{J}(\boldsymbol{\sigma}(\boldsymbol{v}'(t),q'(t))\boldsymbol{n})\|_{L^2(\Gamma)}^2\\
&\qquad+\frac{\rho^s h}{4}\|\boldsymbol{w}(0)-\boldsymbol{\xi}(0)\|_{L^2(\Gamma)}^2+\Delta t^2\rho^s h\|\mathcal{J}(\boldsymbol{\sigma}(\boldsymbol{v}'(0),q'(0))\boldsymbol{n})\|_{L^2(\Gamma)}^2.
\end{aligned}\tag{4.23}$$

Applying equation (3.10), we have

$$\begin{aligned}
&\Delta t^2\rho^s h\|\mathcal{J}(\boldsymbol{\sigma}(\boldsymbol{v}'(t),q'(t))\boldsymbol{n})\|_{L^2(\Gamma)}^2+\Delta t^2\rho^s h\|\mathcal{J}(\boldsymbol{\sigma}(\boldsymbol{v}'(0),q'(0))\boldsymbol{n})\|_{L^2(\Gamma)}^2\\
&\quad\leqslant\frac{\Delta t^4}{\rho^s h}\|\boldsymbol{\sigma}(\boldsymbol{v}'(t),q'(t))\boldsymbol{n}\|_{L^2(\Gamma)}^2+\frac{\Delta t^4}{\rho^s h}\|\boldsymbol{\sigma}(\boldsymbol{v}'(0),q'(0))\boldsymbol{n}\|_{L^2(\Gamma)}^2.
\end{aligned}\tag{4.24}$$

Taking into account (4.23) and (4.24), after collecting like terms, we have

$$\mathcal{E}_e(t) + \int_0^t \mathcal{D}_e(\tau)\,\mathrm{d}\tau \leqslant 3\mathcal{E}_e(0) + \int_0^t \mathcal{E}_e(\tau)\,\mathrm{d}\tau + \Delta t^4 \int_0^t \mathcal{O}_1(\tau)\,\mathrm{d}\tau + \Delta t^4 \mathcal{O}_2.$$

Assuming that $\mathcal{E}_e(0)$ and using the Grönwall's inequality, we obtain

$$\mathcal{E}_e(t) + \int_0^t \mathcal{D}_e(\tau)\,\mathrm{d}\tau \leqslant \Delta t^4 \mathrm{e}^t \left(\int_0^t \mathcal{O}_1(\tau)\,\mathrm{d}\tau + \mathcal{O}_2 \right)$$

which completes the proof. □

5 Numerical results

We investigate the performance of the BOUR method on a two- and three-dimensional examples. In the first example, we compute numerical errors and rates of convergence. The second example is based on modeling blood flow in a common carotid artery under physiological conditions. In both examples, we compare performance of the BOUR method with a couple of other partitioned schemes from the literature, namely the kinematically coupled β scheme [10, 11] and the incremental displacement-correction scheme [20].

5.1 Example 1

We present numerical results on a two-dimensional benchmark problem commonly used to investigate performance of numerical schemes for FSI problems [11, 13, 20]. The problem consists of a pressure wave propagating in a straight channel. The fluid domain is a rectangle $\Omega = [0, 5] \times [0, 0.5]$, which corresponds to the upper half of the channel, while the symmetry boundary conditions are prescribed on the bottom fluid boundary

$$\partial_x u_y = 0, \ u_y = 0 \quad \text{on } y = 0.$$

The top boundary represents a thin, elastic structure. To model the structure elastodynamics, we use a generalized string model

$$\rho_s h \partial_{tt} \eta_y + \frac{Eh}{R^2(1-\sigma^2)} \eta_y - \frac{Eh}{2(1+\sigma)} \partial_{xx} \eta_y = f_y$$

where E is the Young's modulus and σ is Poisson's ratio, with the assumption of zero axial displacement, implying that $u_x = 0$ on Γ. The values of the parameters used in this example are given in Table 1.

At the fluid inlet (left boundary) we prescribe

$$\boldsymbol{\sigma}(\boldsymbol{u}, p)\boldsymbol{n} = \begin{cases} \frac{1}{2} p_{\max} \left(1 - \cos\left(\frac{2\pi t}{t_{\max}}\right)\right) \boldsymbol{n}, & t \leqslant t_{\max} \\ 0, & t > t_{\max} \end{cases} \tag{5.1}$$

where $p_{\max} = 1.3333 \cdot 10^4$ dyne/cm^2 and $t_{\max} = 3$ ms. At the right fluid boundary we set $\boldsymbol{\sigma}(\boldsymbol{u}, p)\boldsymbol{n} = 0$. The problem is solved over the time interval $[0, 14]$ ms. We use $\mathbb{P}_2 - \mathbb{P}_1$ elements for the fluid velocity and pressure, and $\mathbb{P}_2$ elements for the displacement.

Tab. 1: Geometry, fluid, and structure parameters used in Example 1.

Parameter	Value	Parameter	Value
Radius R (cm)	0.5	Wall thickness h (cm)	0.1
Length L (cm)	5	Poisson's ratio σ	0.5
Fluid viscosity μ (g/(cm s))	0.035	Young's modulus E (dyne/cm^2)	$0.75 \cdot 10^6$
Fluid density ρ_f (g/cm^3)	1	Wall density ρ_s(g/cm^3)	1.1

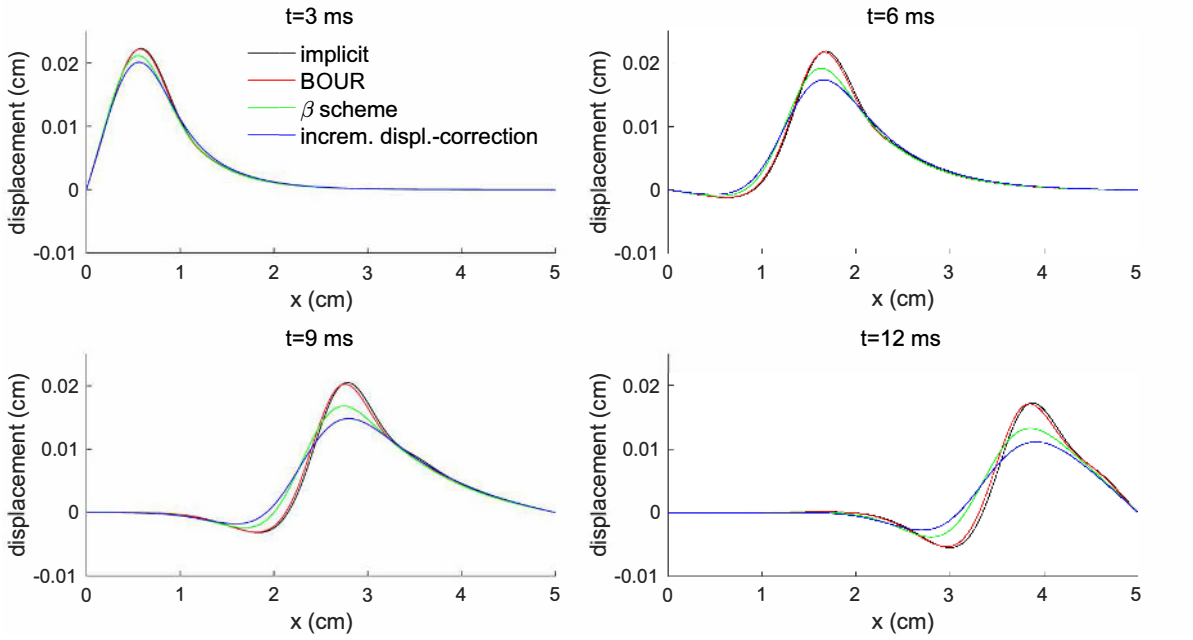

Fig. 2: Structure displacement at $t = 3, 6, 9, 12$ ms obtained using an implicit scheme (black line), BOUR scheme (red line), kinematically coupled β scheme (green line) and incremental displacement-correction scheme (blue line) with $\Delta t = 10^{-4}$ and $\Delta x = 0.02$.

Using this benchmark problem, we compare the performance of the BOUR method to an implicit scheme, the kinematically coupled β scheme [10, 11] and the incremental displacement-correction scheme [20]. The latter two methods are unconditionally stable, first-order partitioned schemes for FSI problems. A second order partitioned method previously developed by the authors in [38] is not included in the comparison because of its time step restrictions. Figure 2 shows the structure displacement, while Figures 3 and 4 show the pressure and the axial velocity in the center of the channel (bottom fluid boundary), respectively. The results are obtained using $\Delta t = 10^{-4}$ and $\Delta x = 0.02$. The BOUR method gives a good agreement with the implicit method. We note that the incremental displacement-correction scheme and the kinematically coupled β scheme dissipate energy much faster than BOUR method.

To investigate the rates of convergence in time, we simultaneously refine spatial and temporal meshes using the following set of parameters

$$(\Delta t, \Delta x) \in \left\{ \frac{5 \cdot 10^{-4}}{2^i}, \frac{5 \cdot 10^{-2}}{2^i} \right\}_{i=0}^{3}. \tag{5.2}$$

Using a reference solution, we compute the relative L^2-error for the fluid velocity and error in the elastic energy-norm for the structure displacement. The reference solution is obtained by solving an implicit scheme with $\Delta x = 5 \cdot 10^{-3}$ and $\Delta t = 5 \cdot 10^{-6}$. On the same example, we compute the errors for the kinematically coupled β scheme and the incremental displacement-correction scheme. Figure 5 shows the comparison of the errors and rates of convergence obtained using the BOUR method (blue line), kinematically coupled β scheme (red line) and the incremental displacement-correction scheme (green line). We observe that the second order convergence is obtained using the BOUR scheme, confirming our theoretical results. Furthermore, when compared to other partitioned schemes, the BOUR scheme exhibits the smallest relative errors.

In order to investigate the convergence using the spatial and temporal parameters of the same order, we change the Young's modulus to $E = 2.5 \cdot 10^2$ dyne/cm^2 and take $p_{\max} = 10$ dyne/cm^2 and $t_{\max} = 0.6$ s in the fluid boundary condition (5.1). The problem is solved over the time interval $[0, 1.2]$ s. All the other parameters are the same as the ones in Table 1. The reference solution is computed using $\Delta x = 6.3 \cdot 10^{-3}$ and $\Delta t = 5 \cdot 10^{-4}$.

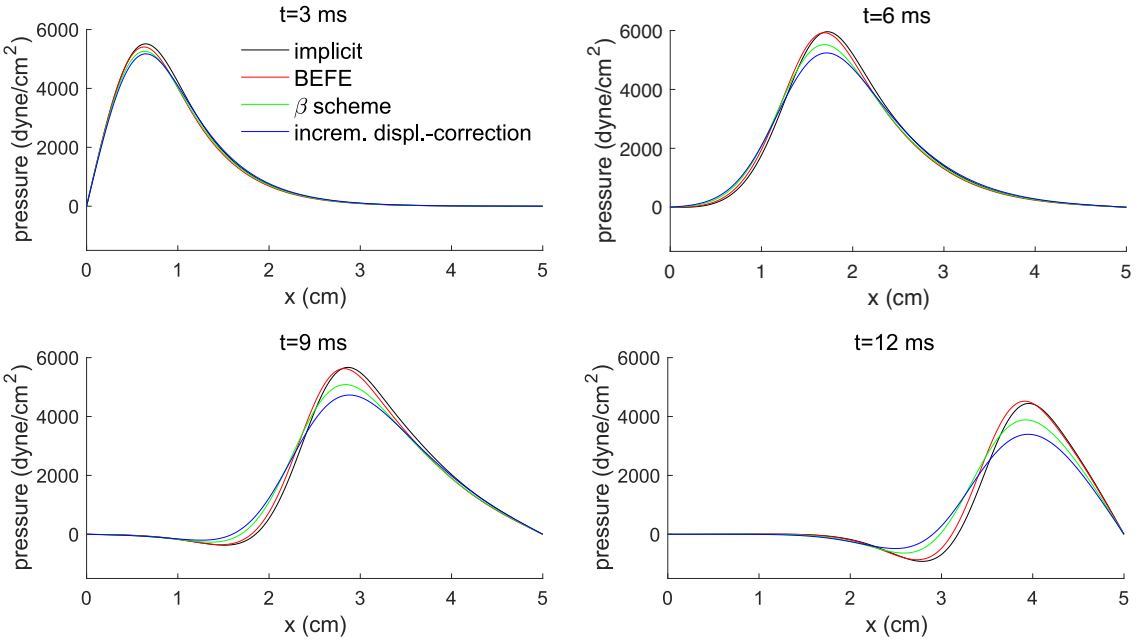

Fig. 3: Pressure in the middle of the channel at $t = 3, 6, 9, 12$ ms obtained using an implicit scheme (black line), BOUR scheme (red line), kinematically coupled β scheme (green line) and incremental displacement-correction scheme (blue line) with $\Delta t = 10^{-4}$ and $\Delta x = 0.02$.

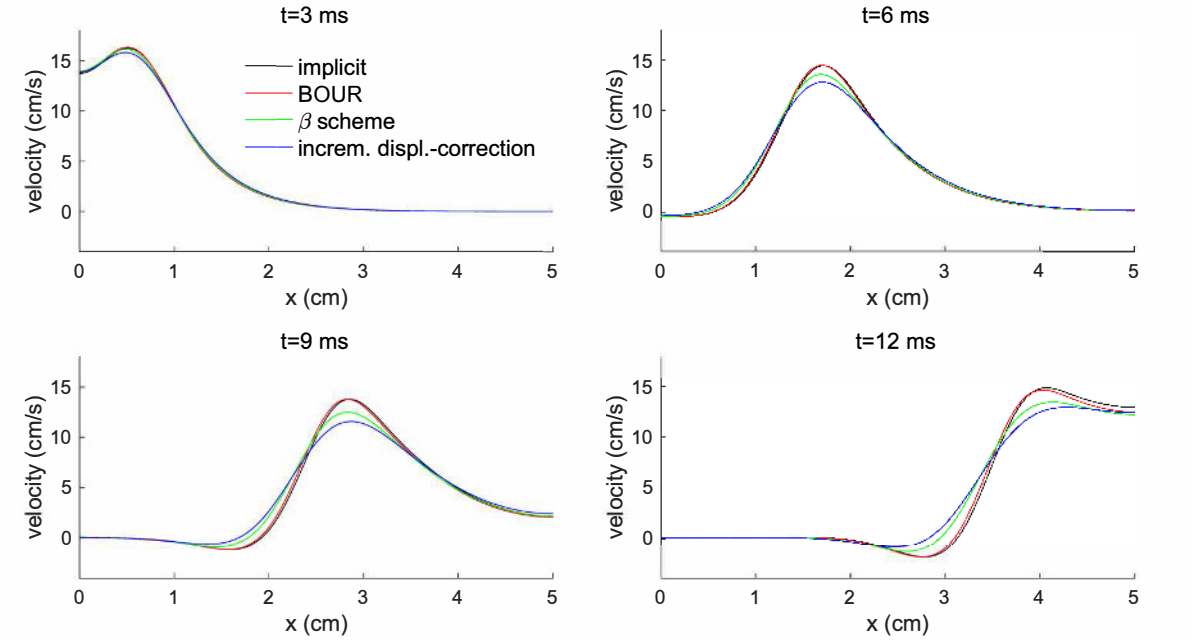

Fig. 4: Axial velocity in the middle of the channel at $t = 3, 6, 9, 12$ ms obtained using an implicit scheme (black line), BOUR scheme (red line), kinematically coupled β scheme (green line) and incremental displacement-correction scheme (blue line) with $\Delta t = 10^{-4}$ and $\Delta x = 0.02$.

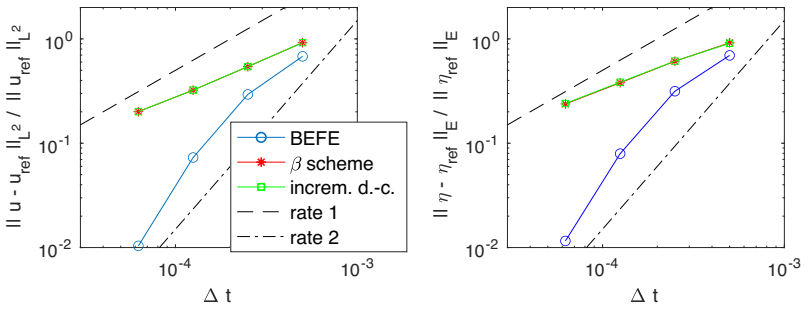

Fig. 5: Relative L^2-errors of the fluid velocity (left) and relative errors in the energy norm for the structure displacement (right) obtained using the BOUR method (blue line), kinematically coupled β scheme (red line), and the incremental displacement-correction scheme (green line) with parameters (5.2).

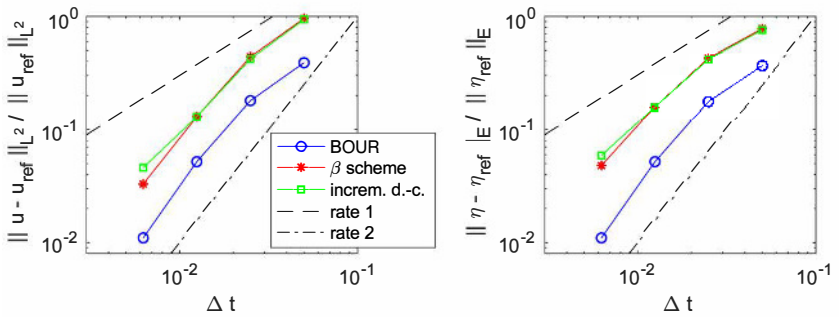

Fig. 6: Relative L^2-errors of the fluid velocity (left) and relative errors in the energy norm for the structure displacement (right) obtained using the BOUR method (blue line), kinematically coupled β scheme (red line), and the incremental displacement-correction scheme (green line) with parameters (5.3).

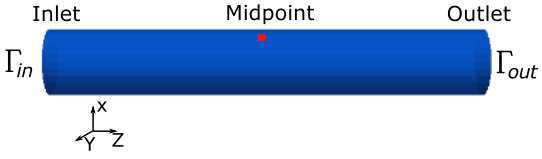

Fig. 7: Computational domain used in Example 2.

The time convergence is investigated using

$$(\Delta t, \Delta x) \in \left\{ \frac{5 \cdot 10^{-2}}{2^i}, \frac{8.3 \cdot 10^{-2}}{2^i} \right\}_{i=0}^{3}. \tag{5.3}$$

Figure 6 shows the comparison of the errors and rates of convergence obtained using the BOUR method (blue line), kinematically coupled β scheme (red line), and the incremental displacement-correction scheme (green line). Again, the BOUR scheme exhibits the smallest relative errors. We notice that in this case, the asymptotic regime is achieved faster them when using parameters (5.2).

5.2 Example 2

In this example we focus on a three-dimensional simplified model of blood flow in common carotid artery. Blood flow is modeled using (2.1) in a straight cylinder of length 4 cm and radius 0.3 cm (see Fig. 7). The fluid lateral boundary represents a thin elastic wall.

Tab. 2: Geometry, fluid, and structure parameters used in Example 2.

Parameter	Value	Parameter	Value
Radius R (cm)	0.3	Wall thickness h (cm)	0.06
Length L (cm)	4	Poisson's ratio σ	0.5
Fluid viscosity μ (g/(cm s))	0.04	Young's modulus E(dyne/cm^2)	$2.6 \cdot 10^6$
Fluid density ρ_f (g/cm^3)	1	Coefficient D_1(dyne/cm^3)	$6 \cdot 10^5$
Wall density ρ_s(g/cm^3)	1.1		

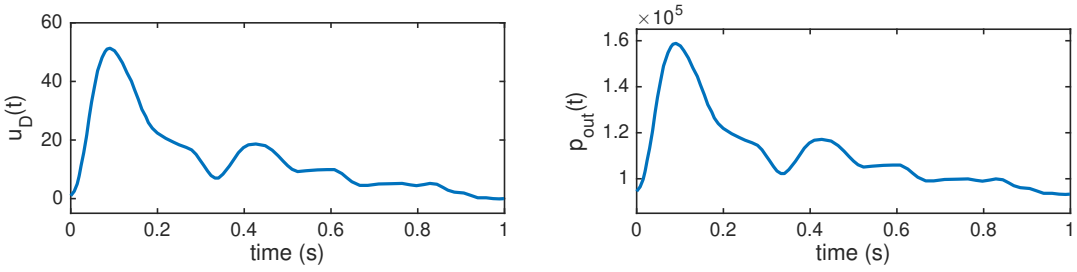

Fig. 8: Boundary conditions for the fluid domain. Left: inlet velocity. Right: outlet pressure.

The wall elastodynamics are modeled using a linear membrane model [16, 23, 24], given in the weak form as

$$\rho_s h \int_\Gamma \frac{\partial^2 \boldsymbol{\eta}}{\partial t^2} \cdot \boldsymbol{\zeta} \, \mathrm{d}S + \underbrace{\int_\Gamma D_1 \boldsymbol{\eta} \cdot \boldsymbol{\zeta} \, \mathrm{d}S + h \int_\Gamma \boldsymbol{\Pi}_\gamma(\boldsymbol{\eta}) : \nabla_\gamma \boldsymbol{\zeta} \, \mathrm{d}S}_{a_s(\boldsymbol{\eta}, \boldsymbol{\zeta})} = \int_\Gamma \boldsymbol{f} \cdot \boldsymbol{\zeta} \, \mathrm{d}S \tag{5.4}$$

where $\boldsymbol{\eta} = (\eta_x, \eta_y, \eta_z)$ denotes the structure displacement. We note that the bilinear form $a_s(\boldsymbol{\eta}, \boldsymbol{\zeta})$ in this case was obtained after operator $\mathcal{L}_s \boldsymbol{\eta}$ was integrated by parts in the equation above. For a linearly elastic, isotropic structure

$$\boldsymbol{\Pi}_\gamma(\boldsymbol{\eta}) = \frac{E}{1+\sigma^2} \frac{\nabla_\gamma \boldsymbol{\eta} + \nabla_\gamma^T \boldsymbol{\eta}}{2} + \frac{E\sigma}{1-\sigma^2} \nabla_\gamma \cdot \boldsymbol{\eta} \tag{5.5}$$

where E denoted the Young's modulus, σ denotes the Poisson's ratio, and $\nabla_\gamma(\cdot)$ denotes the surface gradient, which can be computed as [8, 16]:

$$\nabla_\gamma(\boldsymbol{\eta}) = \nabla \boldsymbol{\eta}(\boldsymbol{I} - \boldsymbol{n} \otimes \boldsymbol{n})$$

where the symbol $\otimes$ denotes the tensor product and $\boldsymbol{I}$ is the identity operator. Term multiplied by D_1 in (5.4) takes into account the constraining effects of the external tissue. Values of the parameters used in this example are given in Table 2.

At the fluid inlet section Γ_{in} we prescribe a fully developed time-dependent axial velocity, and a pressure waveform is imposed at the outlet Γ_{out} using the following boundary conditions [38, 43]:

$$\boldsymbol{u} = \left(0, 0, u_D(t) \frac{R^2 - (x^2 + y^2)}{R^2}\right) \text{ on } \Gamma_{\text{in}}, \qquad \boldsymbol{\sigma n} = -p_{\text{out}}(t)\boldsymbol{n} \text{ on } \Gamma_{\text{out}} \tag{5.6}$$

where $u_D(t)$ and $p_{\text{out}}(t)$ are shown in Fig. 8. All initial conditions are set to zero.

The fluid mesh used in this example consists of 8181 vertices and 41280 tetrahedral elements, while the structure mesh consists of 2268 vertices and 4480 triangles. We used the time step $\Delta t = 10^{-3}$. The problem is solved using the BOUR method, an implicit scheme, the kinematically coupled β scheme, and the incremental displacement-correction scheme. All methods reached a periodic solution after three cardiac cycles.

Figure 9 shows a comparison of the results obtained using different numerical schemes. Left panel shows a comparison of the structure displacement at the midpoint of the structure domain $(0.5, 0, 2)$ and the right panel shows a comparison of the fluid velocity at the center of domain $(0, 0, 2)$. In both cases, the solution

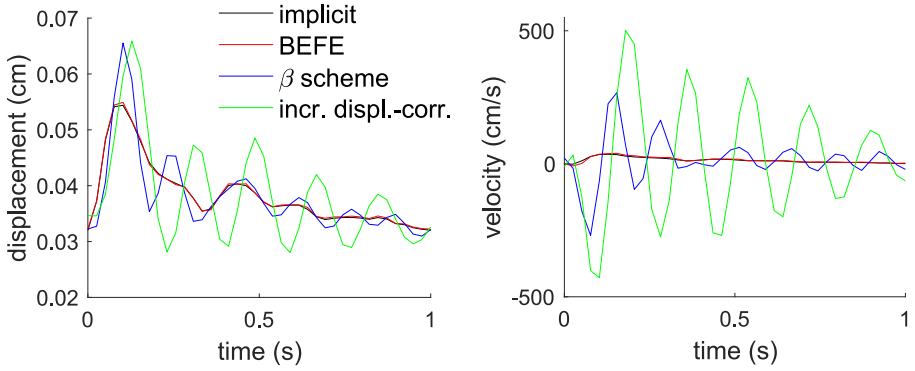

Fig. 9: Comparison of the results obtained using CNFSI scheme and a monolithic scheme. Left: structure displacement. Right: fluid velocity.

obtained with the BOUR method is in an excellent agreement with the solution obtained using an implicit approach. Even though the kinematically coupled β scheme and the incremental displacement-correction scheme gave stable and periodic results, they significantly differ from the solution obtained by the implicit scheme. Due to their lower convergence rate, a much smaller time step would have to be used to get satisfactory results.

6 Conclusions

We proposed and analyzed a novel partitioned method for the interaction between a viscous incompressible fluid and a thin elastic structure. Using energy estimates, we showed that the proposed method is unconditionally stable. Our error analysis indicates that the method is second-order convergent in time. The performance of the scheme is tested on two numerical examples and compared to other schemes available in the literature. While partitioned methods usually require a smaller time step than monolithic methods, our numerical results show a great comparison between the proposed method and the monolithic method using the same time step. This is especially apparent in the second numerical example, where the focus is on modeling blood flow in common carotid artery. In this example, other partitioned schemes consider in this study produced stable, periodic results, but with very poor accuracy when large time steps are used, while the results obtained using the proposed scheme are in an excellent agreement with the results obtained using the monolithic method. The accuracy properties of the proposed scheme and its great performance for large time steps are due to the second-order discretization method used in this study, which is very similar to the midpoint method, and features only a small amount of numerical dissipation. Given its stability, accuracy, and simple implementation, the proposed method is an excellent alternative to the monolithic scheme.

Some limitations of the proposed method are related to the use of a thin structure model and the assumption that the displacement is infinitesimal. Using the second assumption, we further assumed that the fluid domain is fixed, i.e., that the coupling between the fluid and solid sub-problems is linear. The extension of the method to FSI in moving domains will be a subject of our future research.

Funding: The work of the first author was partially supported by the NSF under grants DMS 1912908, DMS 1619993, and DCSD 1934300. The work of the second author was partially supported by the AFOSR under grant FA 9550-16-1-0355 and the NSF under grant DMS 1522574.

Acknowledgment: We would like to thank Fasma Diele (Italian National Research Council, Bari) for helpful discussions on symplectic and geometric integration.

References

[1] S. Badia, F. Nobile, and C. Vergara, Fluid–structure partitioned procedures based on Robin transmission conditions, *J. Comp. Phys.*, **227** (2008), 7027–7051.

[2] S. Badia, F. Nobile, and C. Vergara, Robin-Robin preconditioned Krylov methods for fluid–structure interaction problems, *Comput. Methods Appl. Mech. Engrg.*, **198** (2009), No. 33, 2768–2784.

[3] S. Badia, A. Quaini, and A. Quarteroni, Modular vs. non-modular preconditioners for fluid–structure systems with large added-mass effect, *Comput. Methods Appl. Mech. Engrg.*, **197** (2008), No. 49, 4216–4232.

[4] H. Baek and G. Karniadakis, A convergence study of a new partitioned fluid–structure interaction algorithm based on fictitious mass and damping, *J. Comp. Phys.*, **231** (2012), No. 2, 629–652.

[5] J. Banks, W. Henshaw, and D. Schwendeman, An analysis of a new stable partitioned algorithm for FSI problems. Part I: Incompressible flow and elastic solids, *J. Comp. Phys.*, **269** (2014), 108–137.

[6] J. Banks, W. Henshaw, and D. Schwendeman, An analysis of a new stable partitioned algorithm for FSI problems. Part II: Incompressible flow and structural shells, *J. Comp. Phys.*, **268** (2014), 399–416.

[7] Y. Bazilevs, V.M. Calo, Hughes T.J.R, and Y. Zhang, Isogeometric fluid–structure interaction: theory algorithms and computations, *Comput. Mech.*, **43** (2008), 3–37.

[8] A. Bonito, R. Nochetto, and M. Pauletti, Dynamics of biomembranes: effect of the bulk fluid, *Math. Model. Natur. Phenom.*, **6** (2011), No. 5, 25–43.

[9] H. Brezis, *Functional Analysis, Sobolev Spaces and Partial Differential Equations*, Universitext, Springer, New York, 2011.

[10] M. Bukač, S. Čanić, R. Glowinski, J. Tambača, and A. Quaini, Fluid–structure interaction in blood flow capturing non-zero longitudinal structure displacement, *J. Comp. Phys.*, **235** (2012), 515–541.

[11] M. Bukac and B. Muha, Stability and convergence analysis of the extensions of the kinematically coupled scheme for the fluid–structure interaction, *SIAM J. Numer. Anal.*, **54** (2016), No. 5, 3032–3061.

[12] M. Bukač, I. Yotov, and P. Zunino, An operator splitting approach for the interaction between a fluid and a multilayered poroelastic structure, *Numer. Meth. Partial Differ. Equ.*, **31** (2015), No. 4, 1054–1100.

[13] E. Burman and M. Fernández, Stabilization of explicit coupling in fluid–structure interaction involving fluid incompressibility, *Comput. Methods Appl. Mech. Engrg.*, **198** (2009), 766–784.

[14] E. Burman and M. Fernández, An unfitted Nitsche method for incompressible fluid–structure interaction using overlapping meshes, *Comput. Methods Appl. Mech. Engrg.*, **279** (2014), 497 – 514.

[15] P. Causin, J. F. Gerbeau, and F. Nobile, Added-mass effect in the design of partitioned algorithms for fluid–structure problems, *Comput. Methods Appl. Mech. Engrg.*, **194** (2005), No. 42-44, 4506–4527.

[16] C. M. Colciago, S. Deparis, and A. Quarteroni, Comparisons between reduced order models and full 3D models for fluid–structure interaction problems in haemodynamics, *J. Comp. Appl. Math.*, **265** (2014), 120–138.

[17] W. G Dettmer and D. Perić, A new staggered scheme for fluid–structure interaction, *Int. J. Numer. Methods Engrg.*, **93** (2013), No. 1, 1–22.

[18] D. R. Durran, *Numerical Methods for Fluid Dynamics with Applications to Geophysics*, 2nd ed., Texts in Applied Mathematics, Vol. 32, Springer, New York, 2010.

[19] L. Failer and T. Wick, Adaptive time-step control for nonlinear fluid–structure interaction, *J. Comp. Phys.*, **366** (2018), 448–477.

[20] M. Fernández, Incremental displacement-correction schemes for incompressible fluid–structure interaction: stability and convergence analysis, *Numerische Mathematik*, **123** (2013), No. 1, 21–65.

[21] M. Fernández, J-F. Gerbeau, and C. Grandmont, A projection semi-implicit scheme for the coupling of an elastic structure with an incompressible fluid, *Int. J. Numer. Methods Engrg.*, **69** (2007), No. 4, 794–821.

[22] M. Fernández and J. Mullaert, Convergence and error analysis for a class of splitting schemes in incompressible fluid–structure interaction, *IMA J. Numer. Anal.*, **36** (2016), No. 4, 1748–1782.

[23] A. Figueroa, S. Baek, C. Taylor, and J. Humphrey, A computational framework for fluid–solid-growth modeling in cardiovascular simulations, *Comput. Methods Appl. Mech. Engrg.*, **198** (2009), No. 45, 3583–3602.

[24] C. Figueroa, I. Vignon-Clementel, K. Jansen, T. Hughes, and C. Taylor, A coupled momentum method for modeling blood flow in three-dimensional deformable arteries, *Comput. Methods Appl. Mech. Engrg.*, **195** (2006), No. 41-43, 5685–5706.

[25] D. Forti, M. Bukac, A. Quaini, S. Canic, and S. Deparis, A Monolithic Approach to Fluid–Composite Structure Interaction, *J. Sci. Comp.*, (2016), 1–26.

[26] D. F. Griffiths and J. M. Sanz-Serna, On the scope of the method of modified equations, *SIAM J. Sci. Stat. Comp.*, **7** (1986), No. 3, 994–1008.

[27] D. F. Griffiths and D. J. Higham, *Numerical Methods for Ordinary Differential Equations. Initial Value Problems*, Springer Undergraduate Mathematics Series, Springer-Verlag, 2010.

[28] G. Guidoboni, R. Glowinski, N. Cavallini, and S. Čanić, Stable loosely-coupled-type algorithm for fluid–structure interaction in blood flow, *J. Comp. Phys.*, **228** (2009), No. 18, 6916–6937.

[29] A. Guzel and W. Layton, Time filters increase accuracy of the fully implicit method, *BIT Numer. Math.*, **58** (2018), No. 2, 301–315.

[30] A. Guzel and C. Trenchea, The Williams step increases the stability and accuracy of the hoRA time filter, *Appl. Numer. Math.*, **131** (2018), 158–173.
[31] A. Guzel and C. Trenchea, The Williams step increases the stability and accuracy of the hoRA time filter, *Appl. Numer. Math.*, **131** (2018), 158–173.
[32] E. Hairer, C. Lubich, and G. Wanner, *Geometric Numerical Integration*, Springer Series in Computational Mathematics, Vol. 31, Springer, Heidelberg, 2010.
[33] M. Heil, A. Hazel, and J. Boyle, Solvers for large-displacement fluid–structure interaction problems: segregated versus monolithic approaches, *Comput. Mech.*, **43** (2008), No. 1, 91–101.
[34] W. Hundsdorfer and J. Verwer, *Numerical Solution of Time-Dependent Advection–Diffusion–Reaction Equations*, Springer Series in Computational Mathematics, Vol. 33, Springer-Verlag, Berlin, 2003.
[35] W. Layton, Y. Li, and C. Trenchea, Recent developments in IMEX methods with time filters for systems of evolution equations, *J. Comp. Appl. Math.*, **299** (2016), 50–67.
[36] R. J. LeVeque, *Numerical Methods for Conservation Laws*, 2-nd ed., Lectures in Mathematics ETH Zürich, Birkhäuser Verlag, Basel, 1992.
[37] M Lukáčová-Medvid'ová, G Rusnáková, and A Hundertmark-Zaušková, Kinematic splitting algorithm for fluid–structure interaction in hemodynamics, *Comput. Methods Appl. Mech. Engrg.*, **265** (2013), 83–106.
[38] O. Oyekole, C. Trenchea, and M. Bukac, A Second-Order in Time Approximation of Fluid-Structure Interaction Problem, *SIAM J. Numer. Anal.*, **56** (2018), No. 1, 590–613.
[39] C. S. Peskin, Numerical analysis of blood flow in the heart, *J. Comp. Phys.*, **25** (1977), No. 3, 220–252.
[40] A. Quaini and A Quarteroni, A semi-implicit approach for fluid–structure interaction based on an algebraic fractional step method, *Math. Models Methods Appl. Sci.*, **17** (2007), No. 6, 957–985.
[41] R. D. Ruth, A canonical integration technique, *IEEE Trans. Nucl. Sci.* (1983), 2669–2671.
[42] R. Van Loon, P. D. Anderson, J. De Hart, and F. P. T. Baaijens, A combined fictitious domain/adaptive meshing method for fluid–structure interaction in heart valves, *Int. J. Numer. Methods Fluids*, **46** (2004), No. 5, 533–544.
[43] Z. Wang, N. Wood, and X. Xu, A viscoelastic fluid–structure interaction model for carotid arteries under pulsatile flow, *Int. J. Numer. Methods Biomed. Engrg.*, **31** (2015), No. 5.
[44] R. F. Warming and B. J. Hyett, The modified equation approach to the stability and accuracy analysis of finite-difference methods, *J. Comp. Phys.*, **14** (1974), 159–179.
[45] Y. Yu, H. Baek, and G. Karniadakis, Generalized fictitious methods for fluid–structure interactions: analysis and simulations, *J. Comp. Phys.*, **245** (2013), 317–346.